DESIGN, MODELING AND IMPLEMENTATION OF A SINGLE DIGITAL INPUT BISTABLE MECHANISM

by

Ian Foulds
B.A.Sc., Simon Fraser University, 2003

THESIS
SUBMITTED IN PARTIAL FULFILLMENT OF
THE REQUIREMENTS FOR THE DEGREE OF

MASTER OF APPLIED SCIENCE

In the School
of
Engineering Science

SIMON FRASER UNIVERSITY

February 2004

APPROVAL

Name: **Ian Grant Foulds**

Degree: Masters of Applied Science

Title of Thesis: Design, Modeling and Implementation of a Single Digital Input Bistable Mechanism

Examining Committee:

Chair: **Dr. Glenn Chapman**
Professor
Engineering Science, Simon Fraser University

Dr. Ash Parameswaran
Senior Supervisor
Professor
Engineering Science, Simon Fraser University

Dr. Albert Leung
Examiner
Professor
Engineering Science, Simon Fraser University

Dr. Bonnie Gray
External Examiner
Assistant Professor
Engineering Science, Simon Fraser University

Date Approved: **February 6th, 2004**

PARTIAL COPYRIGHT LICENCE

I hereby grant to Simon Fraser University the right to lend my thesis, project or extended essay (the title of which is shown below) to users of the Simon Fraser University Library, and to make partial or single copies only for such users or in response to a request from the library of any other university, or other educational institution, on its own behalf or for one of its users. I further agree that permission for multiple copying of this work for scholarly purposes may be granted by me or the Dean of Graduate Studies. It is understood that copying or publication of this work for financial gain shall not be allowed without my written permission.

Design, Modeling and Implementation of a Single Digital Input Bistable Mechanism:

Author:

Ian Grant Foulds (Signature)

Feb 18, 2004

(Date Signed)

ABSTRACT

This work presents the first reported single digital input bistable MEMS mechanism. The bistable mechanism is an important building block for many MEMS. Applications of bistable mechanisms to systems such as optical switches, microrelays and motor transmissions, are discussed. Current literature contains examples of dual digital input and single analog input bistable mechanisms; however, no single digital input bistable mechanisms are reported. This work develops the hysteresis spring as an enabling mechanism to allow the creation of the first reported single digital input bistable mechanism. The functionality of the hysteresis spring single digital input bistable mechanism is described and an analytical model is developed. The analytical model is shown to agree, within an acceptable range, with the results of finite element modeling. However, the models are unable to verify the current work due to non-linearity in the operation of the springs in the fabricated devices. Further work to verify the models has been identified. Nevertheless, the proof of concept design has been fabricated and the prescribed functionality has been shown experimentally.

DEDICATION

This work is dedicated to my wife Kristin. Without her support in all arenas of life this work would not have been possible.

ACKNOWLEDGEMENTS

I would like to acknowledge my senior supervisor Dr. Ash Parameswaran who has provided me with support in my endeavors. I would also like to acknowledge Dr. Leung and Dr. Gray for serving on my committee their probing questions forced me to rethink some of my design that I had taken for granted. This work would not have been as readable without the editing efforts of Michael Sjoerdsma. I would also like to acknowledge the rest of my lab group who helped me to refine my presentation.

TABLE OF CONTENTS

LIST OF TABLES

LIST OF FIGURES

LIST OF EQUATIONS

LIST OF ABBREVIATIONS AND ACRONYMS

MEMS – Microelectromechanical Systems

FEA – Finite Element Analysis

1 INTRODUCTION

Microelectromechanical systems (MEMS) are micron scale mechanisms that are fabricated using the techniques developed for the microelectronics fabrication industry. The shared roots of micromachining and microelectronics allow the integration of mechanical and electronic components on the same substrate. This integration makes the concept of "system on a chip" a reality.

For example, in the past, macro-sized accelerometers used to deploy automobile airbags were bulky, expensive and physically separate from the control electronics. The MEMS accelerometers now used in vehicles, integrate the acceleration sensor and control electronics into a single chip. The MEMS accelerometers have a greatly reduced volume and mass, and are less than one fifth [1] the cost of a traditional accelerometer. The automotive industry is not the only sector benefiting from cost savings and performance increase offered by MEMS devices. MEMS are also used extensively to build low-power smart-sensors that are used in many fields such as medicine, chemical processing, communications and defence.

MEMS are batch fabricated using integrated circuit fabrication techniques developed for the electronics industry. Two basic types of micromachining are used to fabricate MEMS: surface micromachining and bulk micromachining [2]. A combination of surface and bulk micromachining is often used take advantage of the strengths of each fabrication technique.

The first method, surface micromachining, is the process of building up a mechanism by depositing layers of thin films on a substrate. The thin film is deposited

and then patterned using photolithography, so that the unwanted portions of the thin film can be etched away. Complex devices can be grown on top of a substrate, by repeating this process of depositing, patterning and etching.

In comparison, bulk micromachining is the process of etching away material from the substrate to produce a device. The substrate is first patterned using photolithographic techniques, after which, the unwanted portions of the substrate are etched away using either isotropic or anisotropic etching methods [2]. By using different sequences of isotropic and anisotropic etching along with patterning, complex devices can be produced from a substrate.

This Master of Applied Science thesis will present my research into a surface micromachined single digital input bistable mechanism.

1.1 Definition of a Bistable Mechanism

A true bistable mechanism is capable of maintaining one of two stable states, and consumes energy only while toggling from one stable state to the other. A common example of such a mechanism is a household light switch. The light switch is stable in either the up or down position and it requires the user to input energy only when flicking the switch. In other words, one does not have to hold the light switch on, as once you have changed the switch's state, the switch will stay in that state. Bistability can be described intuitively through the "ball and hill" example [3] shown in Figure 1.1.

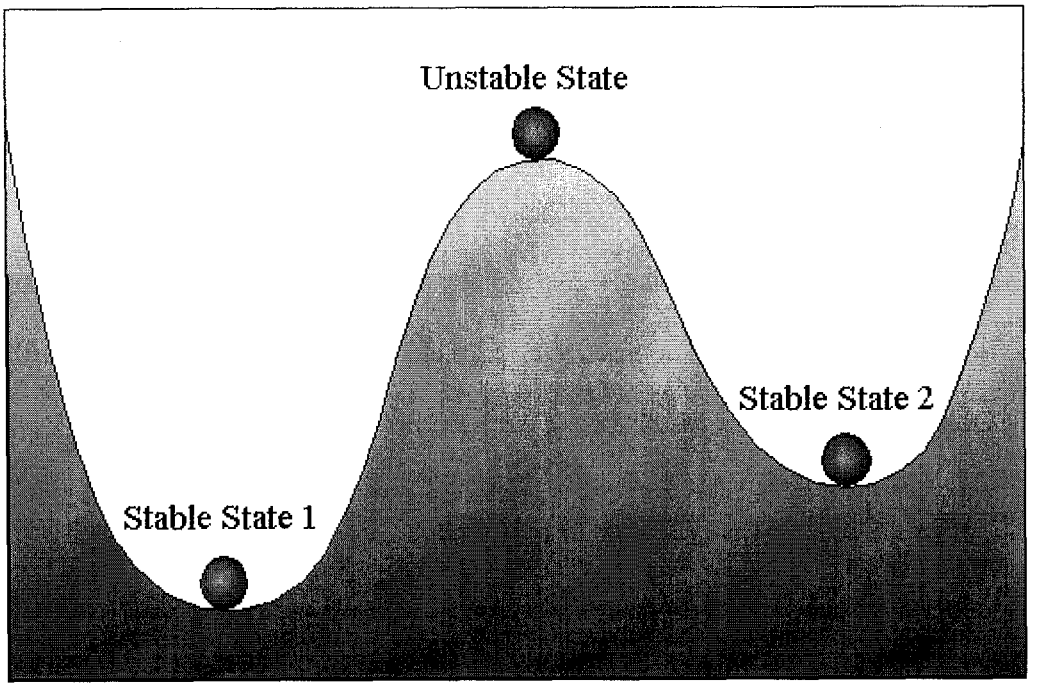

Figure 1.1: Ball and Hill Example of Bistability [i]

The ball is stable in states 1 and 2, meaning that if it is perturbed when in one of these two positions the ball will roll back to its original position because the stable states are the local point of lowest energy. In contrast, when the ball is at the top of the hill, an unstable position, any perturbation will cause the ball to roll and settle in one of the stable states.

To change the state of the ball from position 1 to 2 or vice versa the ball must be actuated over an energy barrier (the hill). Keeping the ball in either stable state requires no energy input and energy is expended only when switching between stable states.

---

[i] Figure by author, based on the cited work.

2 APPLICATIONS OF BISTABLE MECHANISMS

Although the applications of bistable mechanisms are important, this thesis only explores the design of a bistable mechanism itself. However, to provide the reader with an idea of the utility of bistable mechanisms, a description is given in this section of selected applications of bistable mechanisms. The applications discussed are optical switches, microrelays and motor transmissions.

2.1 Optical Switches

Several applications for bistable mechanisms exist in the area of optical switching, such as protection switching and flexible optical add-drop multiplexers. These applications require switches with low insertion loss, low cross talk and bistability, but do not require high speed switching [4]. These criteria can be fulfilled by two main categories of micromachined optical switches: the micromachine aligned fiber switch and the deflection switch.

2.1.1 Micromachine Aligned Fiber Switches

Micromachine aligned fiber switches physically align optical fibers so that the input fiber shines directly into the output fiber. The first reported design, by L.A. Field, [5]et al., shown in Figure 2.1, used two large nickel thermal actuators to push a fiber back and forth in a channel to align it with two output fibers.

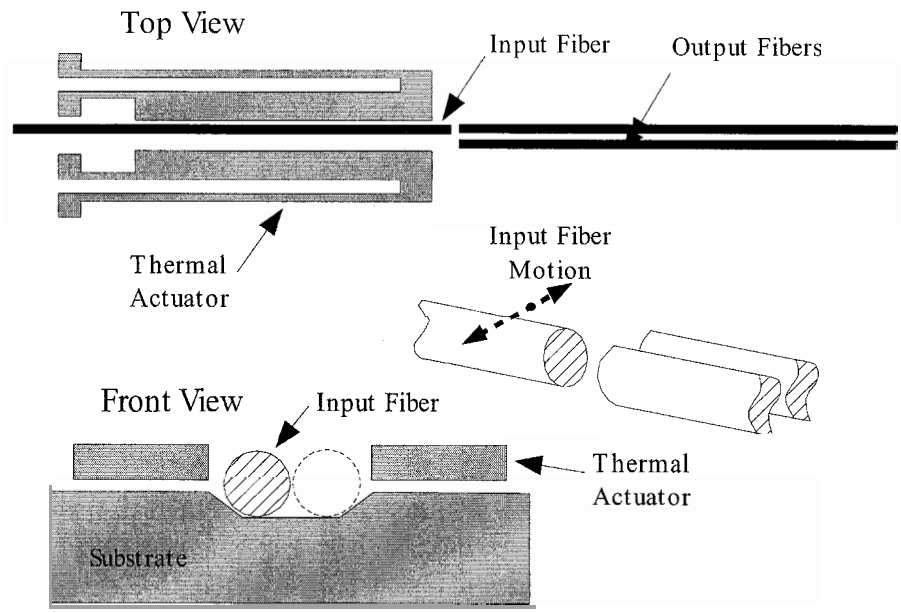

Figure 2.1: First Reported Micromachine Aligned 1x2 Fiber Optic Switch[ii]

This design, while novel, does not enforce bistability or optimal fiber alignment. Soon after this first design was reported, a similar design that used an electrostatically actuated cantilever beam to align waveguides rather than fibers was reported [6]. The waveguide design is illustrated in Figure 2.2.

[ii] Figure by author, based on the cited work.

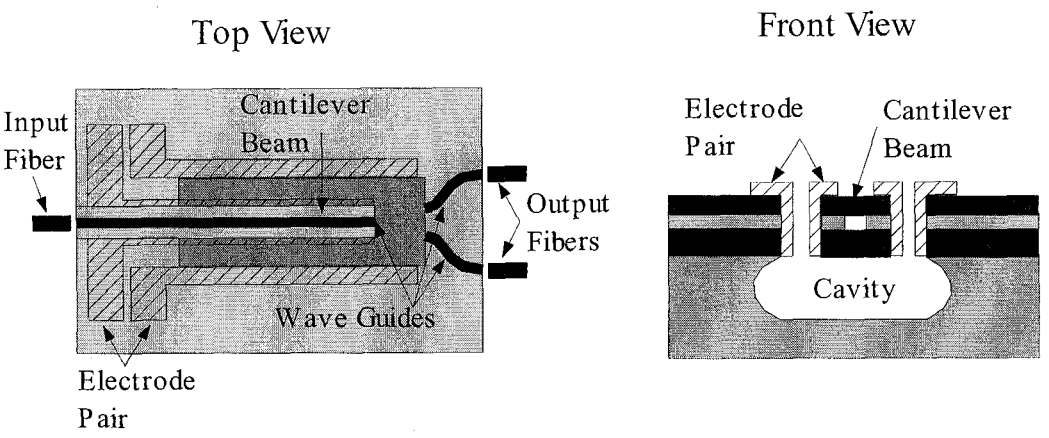

Figure 2.2: Wave Guide Micromachine Aligned Fiber Optic Switch [iii]

The waveguide design has the major disadvantage of not being bistable. To improve on these two designs, the clamped micromachine aligned fiber optic switch was designed by M. Hoffmann, et al [7-11]. The clamped design comes in several different configurations summarized in Figure 2.3.

[iii] Figure by author, based on the cited work.

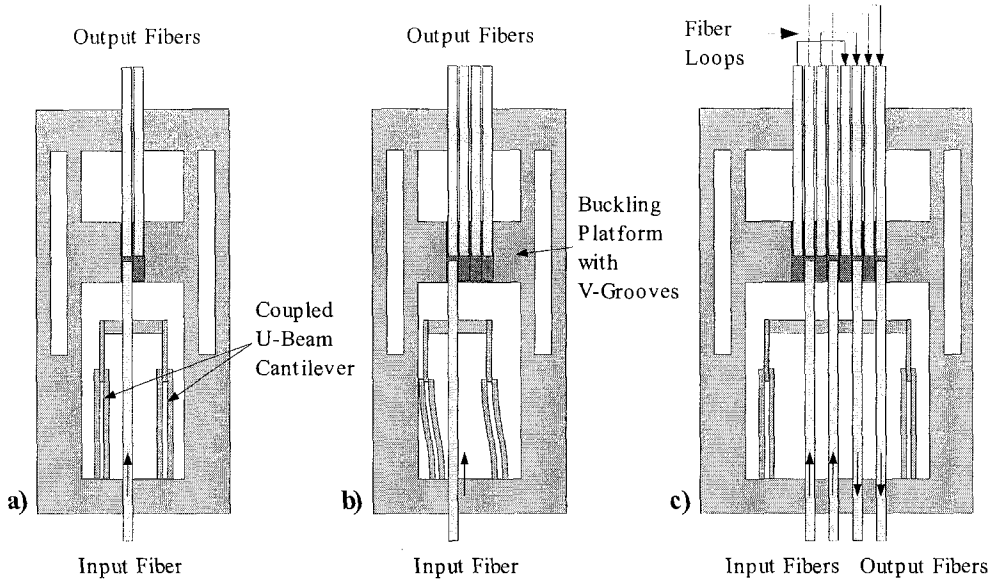

Figure 2.3: Clamped Micromachine Aligned Fiber Optic Switch Configurations a) 1x2 Switch b) 1x4 Switch c) 2x2 Switch [iv]

To understand the basic functionality of the clamped micromachine aligned fiber optic switch, the reader should examine the simple 1 x 2 switch. All other configurations are merely simple extensions of the basic design. The principle of operation is shown in Figure 2.4.

[iv] Figure by author, based on the cited work.

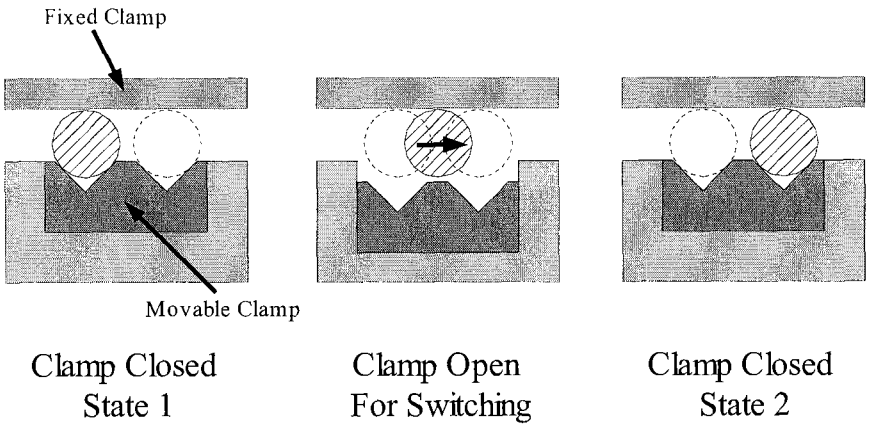

Figure 2.4: Operating Principle of Clamped Micromachine Aligned Fiber Optic Switch [v]

The input and output fibers are held in position with a clamp that consists of a cantilevered platform that moves up and down to press the fibers against a fixed portion. To switch between output fibers, the moving portion of the clamp is bent down to release the input fiber and then the U-beam cantilevers, pictured in Figure 2.3, move the input fiber to align with the second output fiber. The clamp then re-engages, holding the input fiber in place so that the cantilever that moves the input fiber does not need to expend power to hold the input fiber in place. To better align the input fiber to the output fiber, the fibers are placed in v-shaped grooves called fiber guides.

The current method being used to actuate the input fiber in micromachine aligned fiber optic switches, is through heat-based actuators that provide an angular displacement. Because of this use of angular displacement, a slight angular mismatch between the faces of the input and output fibers is created, which degrades the

[v] Figure by author, based on the cited work.

performance of the switch. The use of fiber guide v-grooves helps to limit this angular mismatch, however, switching speed suffers as the angular mismatch between the input fiber and groove increases the settling time of the fiber [11]. Performance of the device could be improved if the input fiber is linearly actuated.

Using a linearly actuated bistable mechanism would address the angular mismatch problems of the current method. As well, using a linearly actuated bistable mechanism would lower the cost by eliminating the need for the fiber clamp, which requires the post processing step of anodic bonding [2].

2.1.2 Deflection Switches

The deflection switch uses mirrors to deflect the light beam from one fiber to another in order to achieve configurable optical transmission. Deflection switches are categorized as either: digital [12-17] or analog [18-20].

The digital deflection switch consists of an array of mirrors that are either on or off, deflecting or not deflecting the light beam respectively. Figure 2.5 depicts a digital deflection optical switch where the mirrors are actuated in-plane to deflect the light beam.

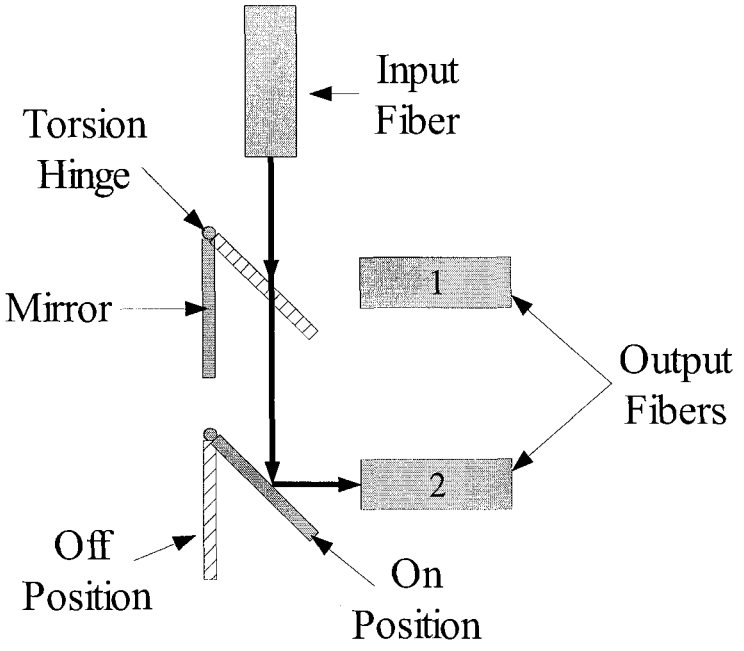

Figure 2.5: An In-Plane Actuated 1x2 Digital Deflection Optical Switch

The 1x2 digital deflection switch depicted in Figure 2.5 shows the lower mirror being on while the upper mirror is off. This configuration allows the light beam to be deflected into the second output fiber. The second configuration shown with hash marks shows the first mirror as on, causing the light beam to be deflected into the first output fiber. In the digital deflection design, each mirror must have two different states; an on state where the light beam is deflected to the target and an off state where the mirror must not interfere with the light beam. For a simple 1x2 switch, the on and off states can be achieved by rotating the mirror around a torsional joint in the plane so that the mirror moves out of the light beam's path. However, when the number of inputs to the switch increases, the mirrors must be actuated out of the plane so that they do not interfere with other light beams. Figure 2.6 depicts a 4x4 Digital Deflection Optical Switch Array.

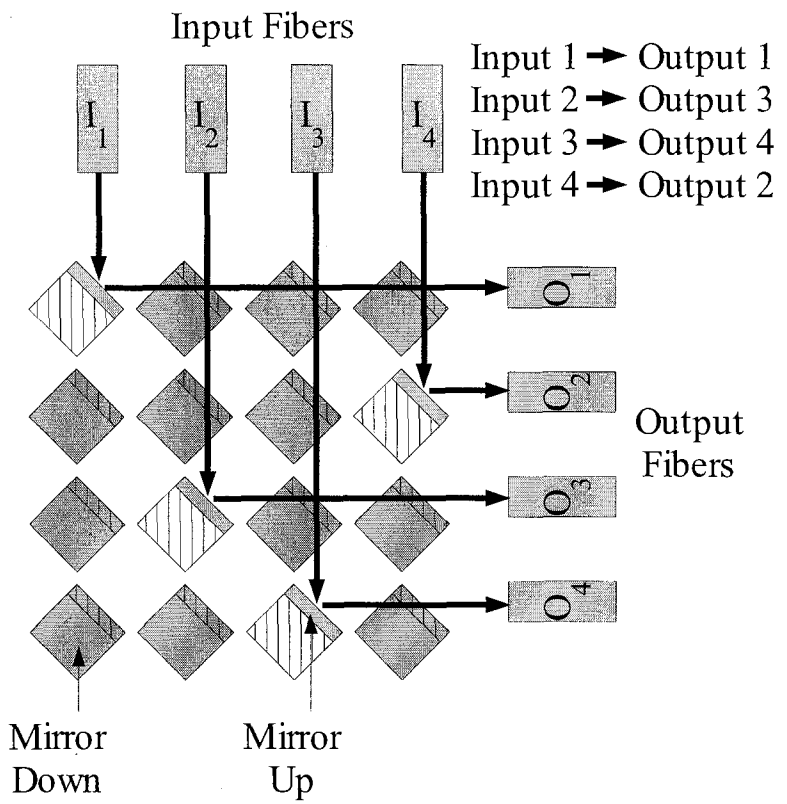

Figure 2.6: A 4x4 Digital Deflection Optical Switch Array

For the 4x4 Digital Deflection Optical Switch Array, the mirrors that are off must be actuated out of the plane so that they do not unintentionally block any optical paths. Because each mirror can only be in one of two states, the digital deflection switch requires M×N mirrors for an MxN switch. As a result of this relationship, the number of mirrors required grows exponentially as the number of inputs increases (M is usually equal to N). Larger numbers of active elements increases the likelihood of a failure and lowers yield.

The second deflection design type is the analog deflection switch. The analog deflection switch consists of one mirror for every input and output. The input mirror is controlled in an analog manner to deflect the light beam to the chosen output mirror,

which in turn deflects the light beam into the output fiber. Figure 2.7 depicts the operation of a 1x2 analog deflection switch.

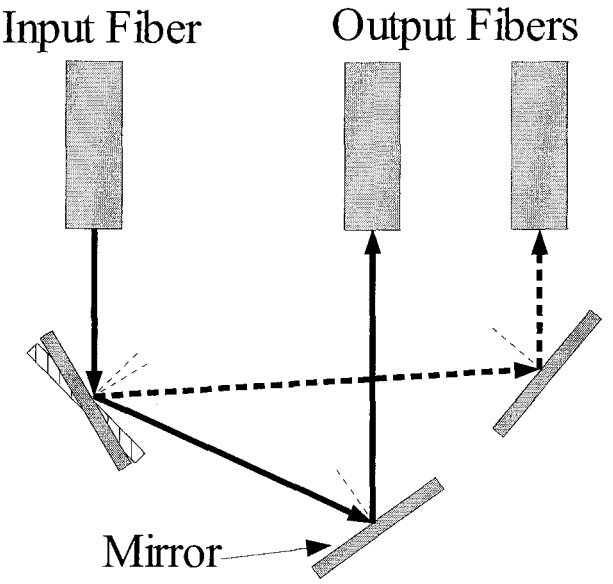

Figure 2.7: A 1x2 Analog Deflection Optical Switch

In Figure 2.7, the configuration shown in solid grey illustrates how the input mirror deflects the beam to the mirror for the first input, which in turn deflects the light beam so that the beam strikes the first output fiber normal to fiber's surface. The second configuration, shown with hash marks, shows how the input mirror rotates to deflect the beam to the second output mirror. Although this simple configuration uses more mirrors than the digital equivalent, it allows each mirror to take on more than two possible states, thus reducing the number of required mirrors for an MxN switch to M+N. This creates a linear relationship between the number of mirrors required and the number of inputs (M is usually equal to N). Because the relationship is linear as the number of inputs increase, the number of mirrors required for a large analog design is much less than that of a digital

design. Figure 2.8 shows a 4x4 analog deflection optical switch, which requires only 8 mirrors instead of 16 for the corresponding digital design.

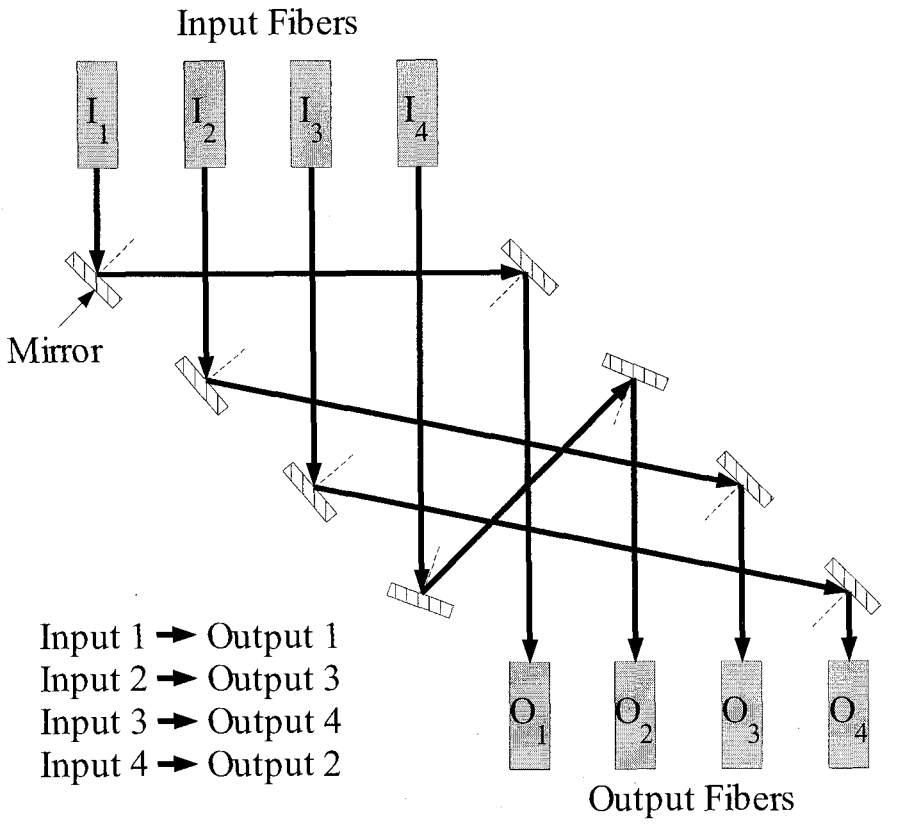

Figure 2.8: A 4x4 Analog Deflection Optical Switch

The decrease in required elements from the digital to analog design comes at the cost of an increased control burden. The digital design requires only digital logic to control the mirrors, where as the analog design requires each mirror to be able to take on many different states. The trade-off of control complexity for number of mirrors must be considered by the optical switch designer when choosing which design type to use.

The bistable mechanism is only useful for very small sized deflection optical switches. For larger switches, either a multistable mechanism or continuous power consumption is required.

2.2 Relays

Mechanical relays are devices that use small currents or voltages to physically connect or disconnect electrical contacts in order to complete or interrupt a circuit. Bistable behaviour is preferred in a relay so that energy is not wasted while maintaining a connection. Relays find many applications in MEMS and several different bistable microrelays have been presented in the literature. A diverse set of design concepts have been shown starting with a liquid metal design [21] as seen in Figure 2.9.

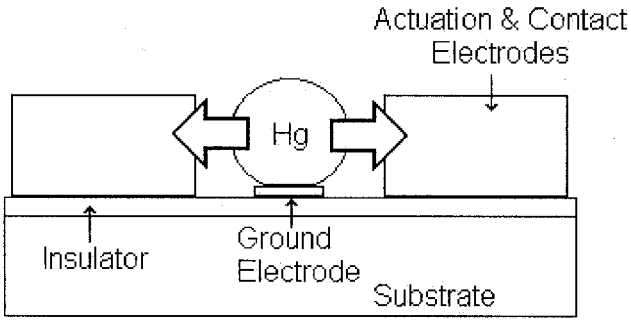

Figure 2.9: Liquid Metal Relay [vi]

The liquid metal relay uses electrostatics to actuate a droplet of mercury and make an electrical contact. The bistable mechanism utilized in the liquid metal relay will be discussed in more depth in section 3.2.3. Another relay reported in the literature uses the thermal actuation of a two-sectioned cantilever to make and break an electrical contact

[vi] Figure by author, based on the cited work.

[22]. This cantilever relay is illustrated in Figure 2.10 and the bistable operation is discussed in detail in section 3.2.1.1.

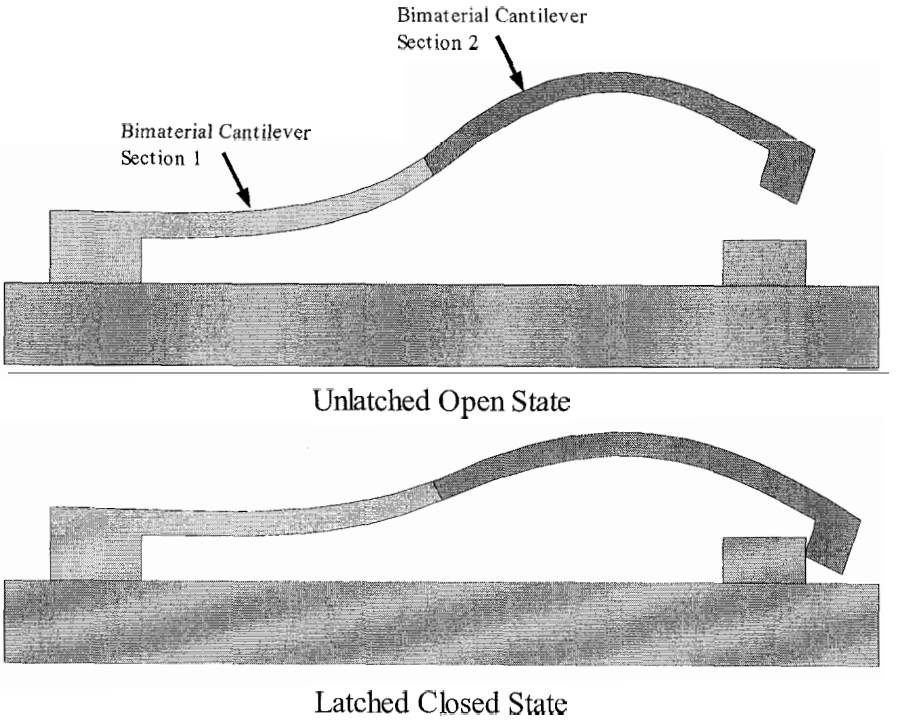

Figure 2.10: Two-Sectioned Cantilever Relay [vii]

A third type of relay reported uses magnetic forces [23], and is illustrated in Figure 2.11.

[vii] Figure by author, based on the cited work.

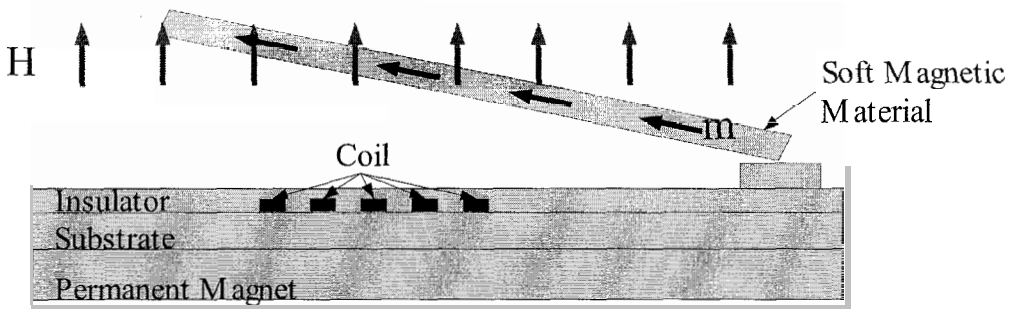

Figure 2.11: Magnetic Relay [viii]

The magnetic relay relies on both soft and hard magnetic materials to provide a bistable contact. The bistable mechanism used in the magnetic relay will be discussed in more detail in section 3.2.2.

The reported relays require large chip areas and none has a single digital input. A scalable bistable mechanism with a single digital input could easily find application in relay designs.

2.3 Micromotor Transmission

Motors are an important part of many MEMS designs. Often, due to the fabrication process being utilized, the most practical type of motor to use is the unidirectional motor called a pawl and ratchet. The pawl and ratchet motor can be designed using only a single input, an example of which is illustrated in Figure 2.12.

[viii] Figure by author, based on the cited work.

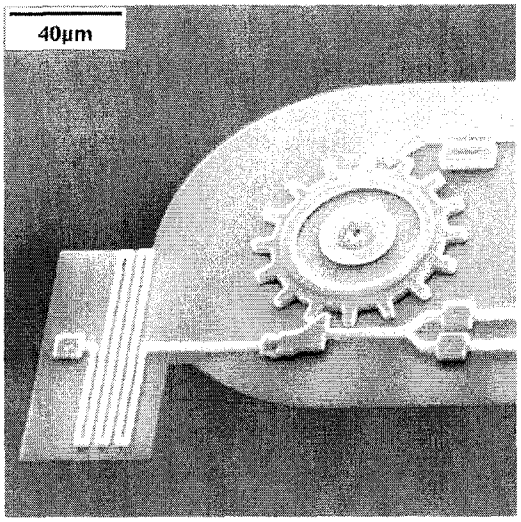

Figure 2.12: Pawl and Ratchet Motor Designed at Simon Fraser University (SFU)[ix]

The simple functionality of this motor can be extended from a unidirectional motor into bi-directional motor through the switching of gear trains. This extension can be achieved by creating a motor transmission that can engage either a forward or reverse gear train to the motor. Figure 2.13 shows such a transmission.

[ix] This SEM picture used with permission of the IMMR at Simon Fraser University www.sfu.ca/immr

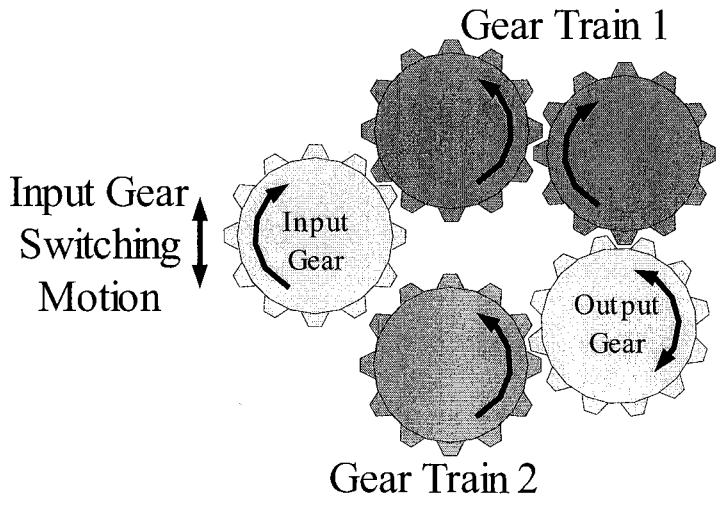

Figure 2.13: Model of MEMS Motor Transmission

As shown in the model, when the input gear is attached to output gear train 1, the output gear rotates counter-clockwise; where as, when the input gear is attached to output gear train 2, the output gear rotates clockwise. Thus, the output gear can be rotated in either direction by switching the motor from one gear train to the other. Figure 2.14 shows a MEMS motor transmission that was designed at SFU. Note that the moving gear in this design is not the motor gear but an intermediate gear. This was done to keep the design of the actual motor as simple as possible.

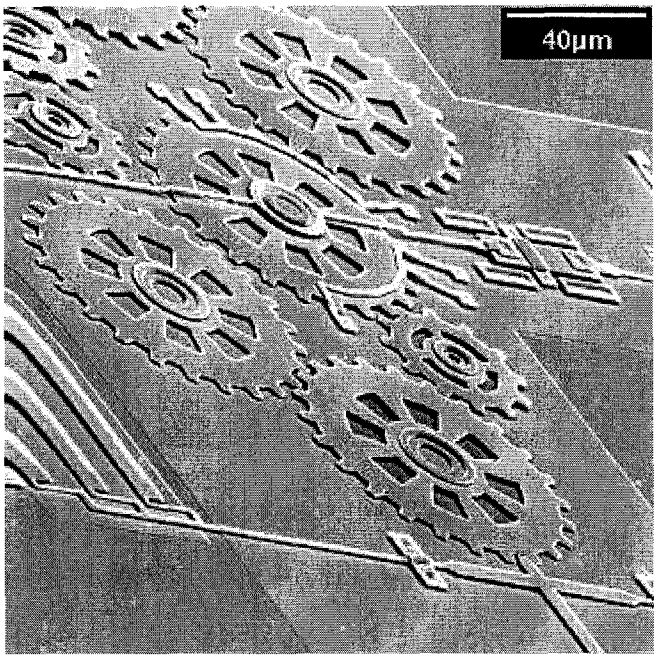

Figure 2.14: MEMS Motor Transmission Designed at SFU [x]

The use of a single digital input bistable mechanism in MEMS motor transmissions would allow for unidirectional pawl and ratchet motors to be extended to bi-directional functionality at the cost of only one more input.

Micro-transmissions can also be used to extend the use of any micro motor by using gear train switching to allow a single motor to drive multiple devices. This functional extension could be accomplished by not tying the gear trains to the same output gear but to different output gears that drive separate devices. Thus, through the use of gear train switching, a bistable mechanism could be used to allow a motor to drive two separate devices saving both fabrication area and input pins.

---

[x] This SEM picture used with permission of the IMMR at Simon Fraser University www.sfu.ca/immr

3 BISTABLE MECHANISMS IN THE LITERATURE

Several bistable mechanisms are reported in the literature, all of which can be categorised into two basic types: compliance-based mechanisms and noncompliant mechanisms.

The compliance-based mechanisms use a strategy of requiring a spring to be compressed while transitioning between states, which creates an energy barrier between states and results in a snapping motion. Energy is stored in the spring until the mechanism is actuated beyond the threshold between states. Once the mechanism has been actuated beyond the threshold, the energy in the spring is released, bringing the mechanism into its second stable state.

The noncompliant mechanisms, in comparison use various strategies such as: locking mechanisms, permanent magnetic fields and electrostatics to achieve bistable behaviour.

3.1 Compliance-Based Mechanisms

3.1.1 Classic Compliance-Based Design

Brian Jenson, et al. reported a classic compliance-based bistable mechanism [24]. Their design is illustrated in Figure 3.1.

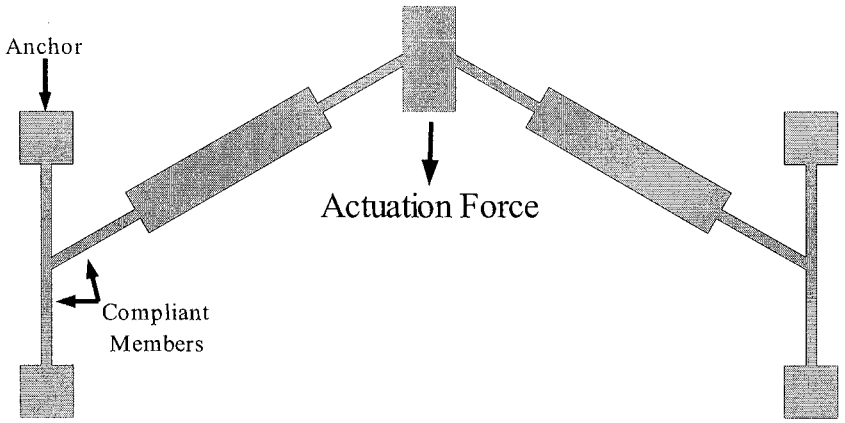

Figure 3.1: Schematic of Classic Compliance-based Bistable Mechanism [xi]

The operating principle of this design is most easily understood by examining its rigid body model. The rigid body model for the classic compliance-based bistable mechanism is depicted in Figure 3.2.

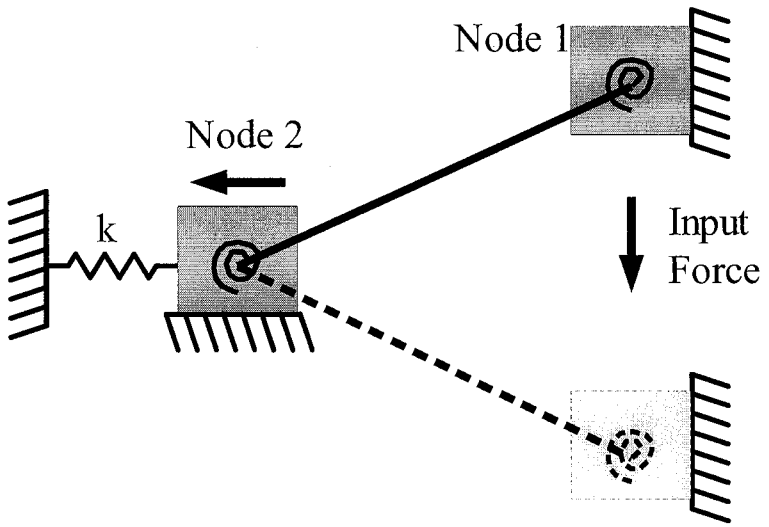

Figure 3.2: Rigid Body Model of Classic Compliance-based Device [xii]

[xi] Figure by author, based on the cited work.

[xii] Figure by author, based on the cited work.

The rigid body model shown in Figure 3.2 can be mirrored to provide the layout shown in Figure 3.1. The classic device operates as follows. As node 1 is forced downward, node 2 is forced to the left because of the constraints that have been placed on them. This motion stores energy in the spring k and creates the energy barrier between the two states. Once node 1 is lower than node 2, the energy barrier has been overcome and node 1 snaps into its second stable position indicated by the dashed lines.

One of the main constraints for the operation of this device is that the energy required to compress the lateral spring must be greater than the energy stored in the torsional springs at the nodes. If the torsional springs store more energy than is required to compress the lateral spring, the device will not be stable in the lower state, because the torsional springs would then have more energy than the barrier energy provided by the lateral spring causing the device to snap back to its original stable state.

Note that this device requires two distinct inputs to allow actuation between states. Further, the distance between stable states is quite minimal in relation to the footprint of the entire device.

3.1.2 Centrally Clamped Parallel-Beam

J. Qui, et al. designed the next device depicted in Figure 3.3 [25]. This device is a clamped parallel-beam snapping bistable mechanism.

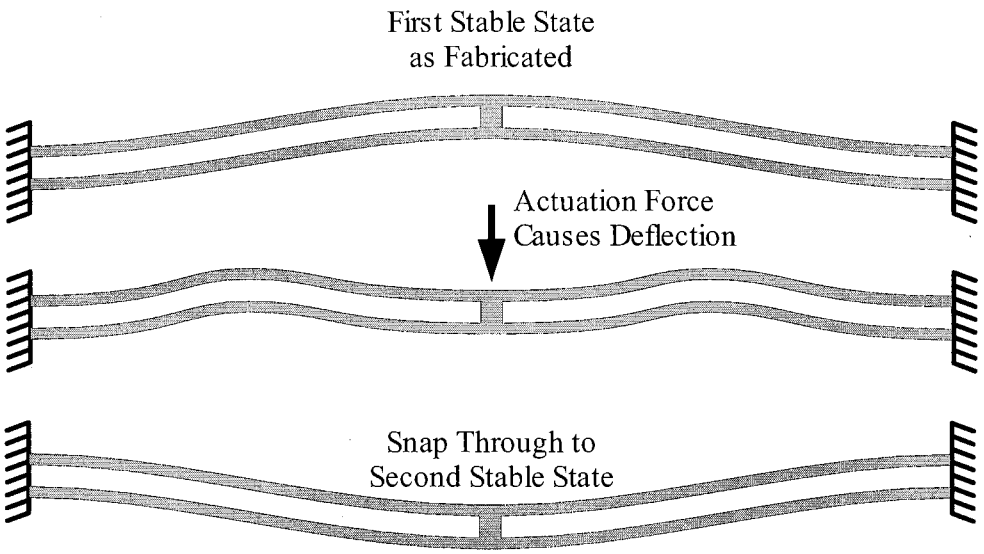

Figure 3.3: Centrally Clamped Parallel-Beam Bistable Mechanism [xiii]

The device is fabricated in its first stable state. To reach a second stable state the clamped beam is actuated at the center of the beam until its switching threshold has been exceeded, at which point the beam snaps through into its second stable state. The central clamp is essential to the operation of this device as it allows only the first and third deflection modes to occur. The second and third deflection modes both lower the energy barrier between stable states, the second mode lowers the energy barrier to a greater degree than the third mode. The result is that if the second mode is allowed to occur in this type of device, bistable behavior is not achievable.

This device, as reported, has the disadvantage of being 3 mm long and almost 0.5 mm deep. A second disadvantage of this device is that it requires actuation in two different directions to switch between stable states. To transition from the first state to

---

[xiii] Figure by author, based on the cited work.

the second state the clamped beam must be actuated towards the second state. To return to the first state, the clamped beam must be actuated towards the first state.

J. Qiu, et al., having designed a bistable mechanism, chose to utilize their mechanism as the main design block of a microrelay [26]. Their microrelay design is depicted in Figure 3.4.

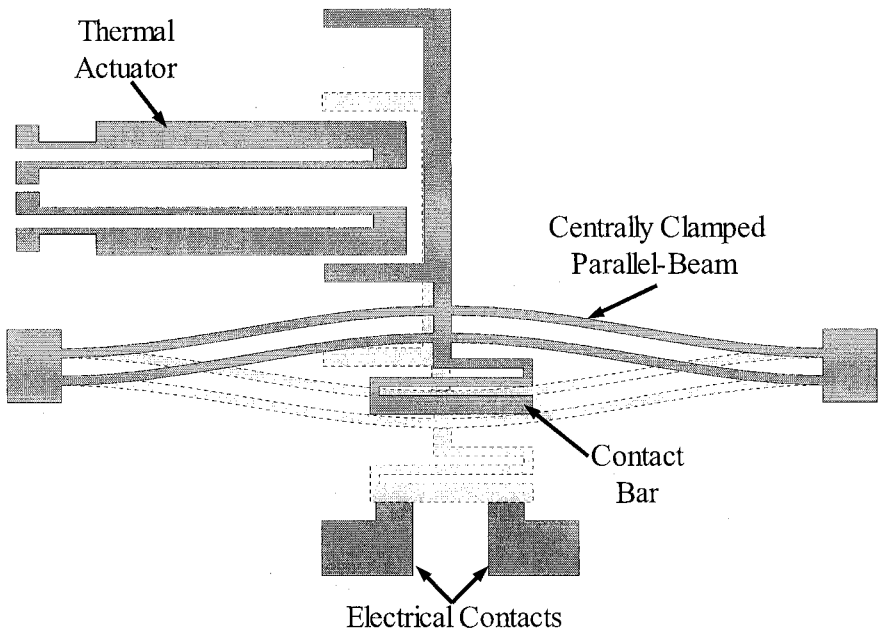

Figure 3.4: Microrelay Utilizing the Centrally Clamped Parallel-Beam Bistable Mechanism [xiv]

To create a microrelay J Qiu, et al. used the centrally clamped parallel-beam as the main design block, attached actuation to one side of the parallel beam and a contact bar to the other side. The device is fabricated in an off state and is switched between states using thermal actuators.

[xiv] Figure by author, based on the cited work.

This relay is a good example of how a bistable mechanism is a mechanical building block that can be combined with other basic blocks such as actuators and contacts to create a useful device.

3.1.3 Snapping Actuator

The snapping actuator design by H. Matoba, et al. [27] uses the same principles as all of the compliance-based bistable mechanisms; however, the actuation is integrated with the body of the mechanism. As shown in Figure 3.5, this device has three inputs: one input to actuate from the first stable state to the second stable state; a second input for the reverse process; and a third input to lower tension in the spring that creates the energy barrier between states.

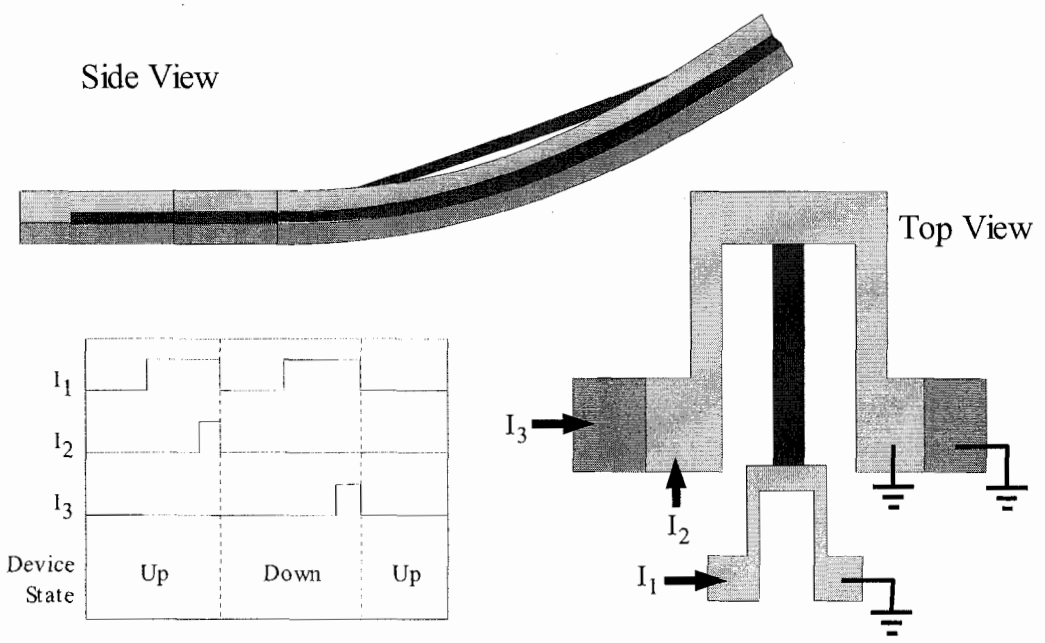

Figure 3.5: Schematic of Snapping Actuator and Timing Diagram [xv]

[xv] Figure by author, based on the cited work.

In this design, actuation between states is achieved through the use of differential heating. When the actuator is in the up state, heating the upper polysilicon U-shaped cantilever causes the top layer to expand, which causes the device as a whole to want to curl downward. When the force created by the differential heating exceeds the force being applied by the tension spring, the energy barrier has been overcome and the actuator snaps into the down state. The device can then be returned to an up state by heating the lower polysilicon layer.

This device has the advantage of integrating the actuation of the device into the device itself. As well, this device was reported at a minimum size of 40 μm, which is quite good in comparison with other reported devices. However, this device delivers out of plane displacement and requires a non-standard fabrication process, thus limiting its uses for surface micromachining.

3.1.4 Young Mechanism

The last bistable mechanism in the compliance-based category is the Young mechanism developed at Brigham Young University by B. Jenson, et al [28]. Figure 3.6 shows the two stable states of two different Young mechanisms. A Young mechanism has two rotational joints, two compliant segments and resembles a four bar mechanism. Its bistable behavior is derived in the same way as the other compliance-based designs. As the Young mechanism is rotated about its hubs, the compliant segments store energy. The energy stored in the compliant segments at the second stable state is less than the energy stored in the compliant segments at some threshold between stable states, which creates an energy barrier between stable states.

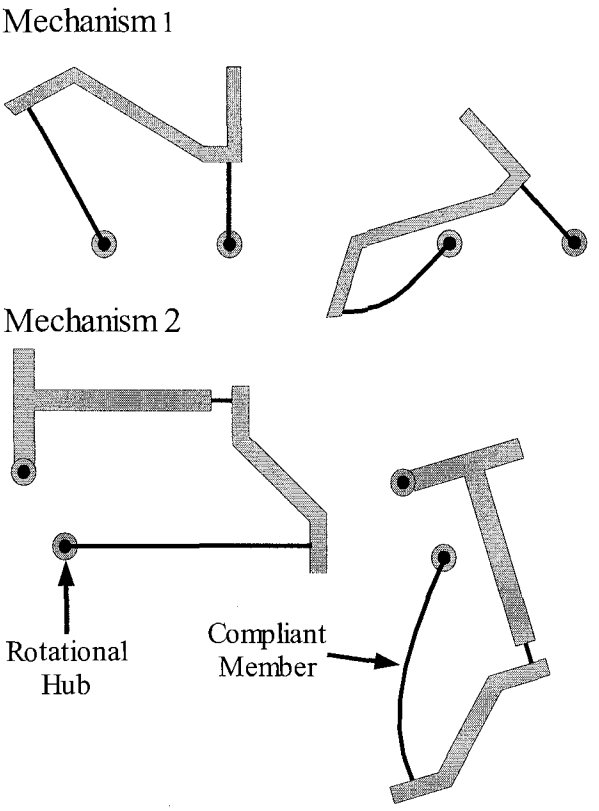

Figure 3.6: Two Examples of a Young Mechanism's Stable States [xvi]

As with all of the compliance-based designs, the Young mechanism has the disadvantage of requiring two inputs for actuation between the stable states. The Young mechanism has the added disadvantage of using rotational hubs, which increase the minimum size and lowers the reliability of the device.

[xvi] Figure by author, based on the cited work.

3.2 Non-Compliant Mechanisms

3.2.1 Latching

3.2.1.1 Multimorph Cantilever

The first noncompliant design discussed is the two-segment multimorph cantilever designed by Xi-Qing Sun, et al. [22].

A bimorph cantilever consists of two layers with different thermal expansion coefficients, which cause the cantilever to bend when heated. The two-segment multimorph cantilever, an extension of the bimorph concept, integrates two bimorph cantilevers into a single cantilever allowing for a more complex motion of the cantilever tip.

To achieve bistable behavior, this design utilizes the ability to control the displacement of the multimorph cantilever's tip. The tip of the cantilever is fashioned into a hook shape and an opposing hook shape is fabricated on the substrate. By using the two inputs to control the position of the cantilever tip, the opposing hooks can be caused to latch. Figure 3.7 shows the motion of the multimorph cantilever as it switches states.

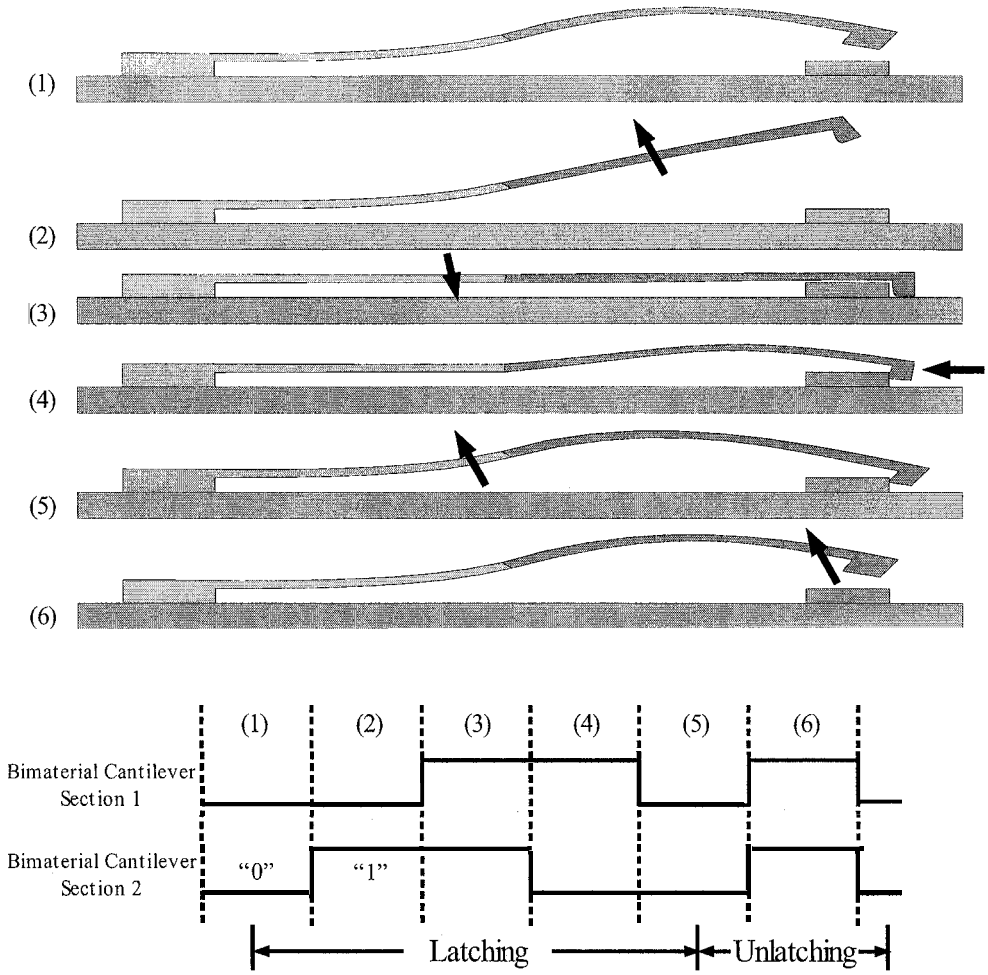

Figure 3.7: Functional View of Two-Segment Multimorph Cantilever [xvii]

When not latched in the on state, the tip of the multimorph cantilever sits above the surface of the substrate and is not in contact with the substrate hook. This configuration is due to the residual stresses imparted during fabrication and is controlled through the choices of bimorph materials, process parameters and structural layout.

[xvii] Figure by author, based on the cited work.

The multimorph cantilever was developed specifically for application as a micro relay. This cantilever has the advantage of including the actuators into the structure of the mechanism, but like the compliance-based mechanisms, it requires two separate inputs for operation. Unfortunately the device uses a non-standard fabrication process and has a large footprint measuring 860μm x 100μm.

3.2.1.2 Extension Ladder Bistable Mechanism

The second latching design to be discussed is the extension ladder bistable mechanism. The first version of this mechanism was designed for my undergraduate thesis [29, 30]. This design, shown in Figure 3.8, is based on the latching mechanism of an extension ladder.

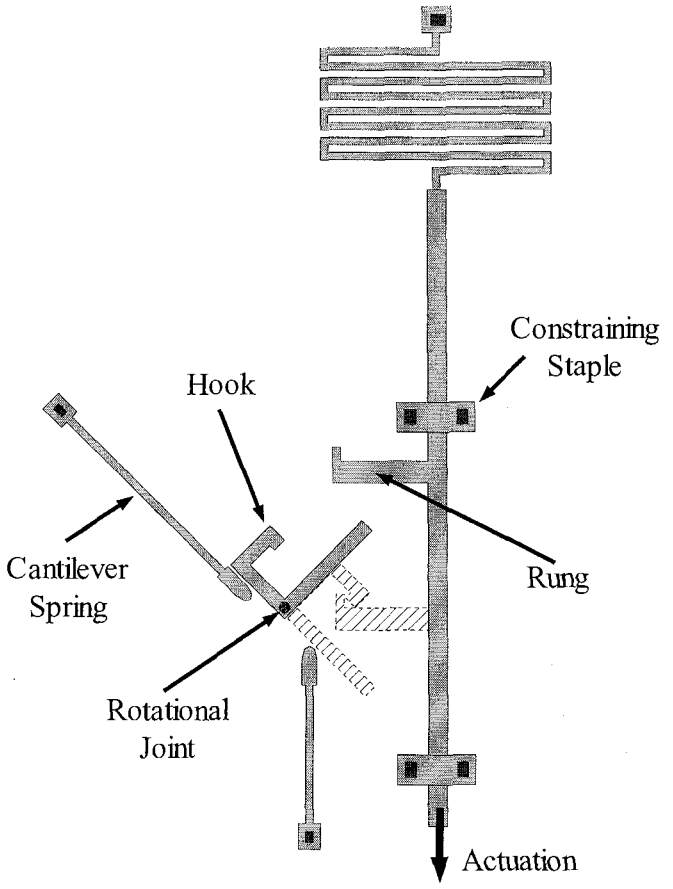

Figure 3.8: Extension Ladder Bistable Mechanism [xviii]

This design is actuated in-plane. The first stable state is the fabricated state depicted in Figure 3.8 as the grey structure. The second stable state occurs when the hook and rung are latched, which is depicted as the hash-marked structures in Figure 3.8.

Two thresholds govern the operation of the extension ladder bistable mechanism. The mechanism will enter the second stable state if the rung is actuated beyond the first

[xviii] Figure by author, based on the cited work.

threshold, but not beyond the second threshold. The mechanism enters the first stable state if the rung is either not actuated beyond the first threshold, or if it is actuated beyond the second threshold. Normal operation, depicted in Figure 3.9, involves actuating the rung beyond the first threshold to latch the mechanism in its second stable state. The rung is then actuated beyond the second threshold to unlatch the mechanism and return it to its original stable state. Actuating the rung from the first stable state past the second threshold would result in the mechanism undergoing no change of state.

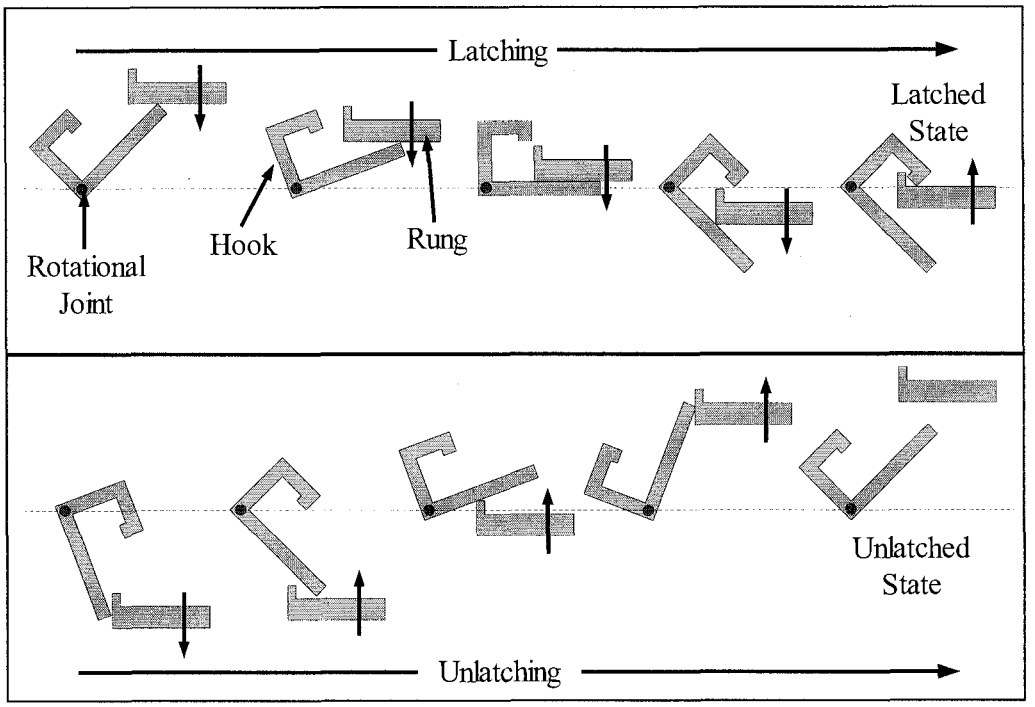

Figure 3.9: Latching and Unlatching Motion of the Extension Ladder Bistable Mechanism

The extension ladder bistable mechanism has the advantage of requiring only a single analog input. As well, the extension ladder design can be made into a multistable mechanism by adding additional rungs. Although adding rungs will increase the number

of thresholds, which obviously complicates the control of the input, adding the rungs extends the design to be multistable without increasing the number of inputs required.

One of the disadvantages of the extension ladder design is the use of a rotational joint for the hook. Rotational joints increase the minimum size of the design and are less reliable than a compliant joint. Therefore, further work was undertaken to design an extension ladder based mechanism that approximates the function of a rotational joint with a compliant joint. The basic layout for the compliant extension ladder based design is shown in Figure 3.10.

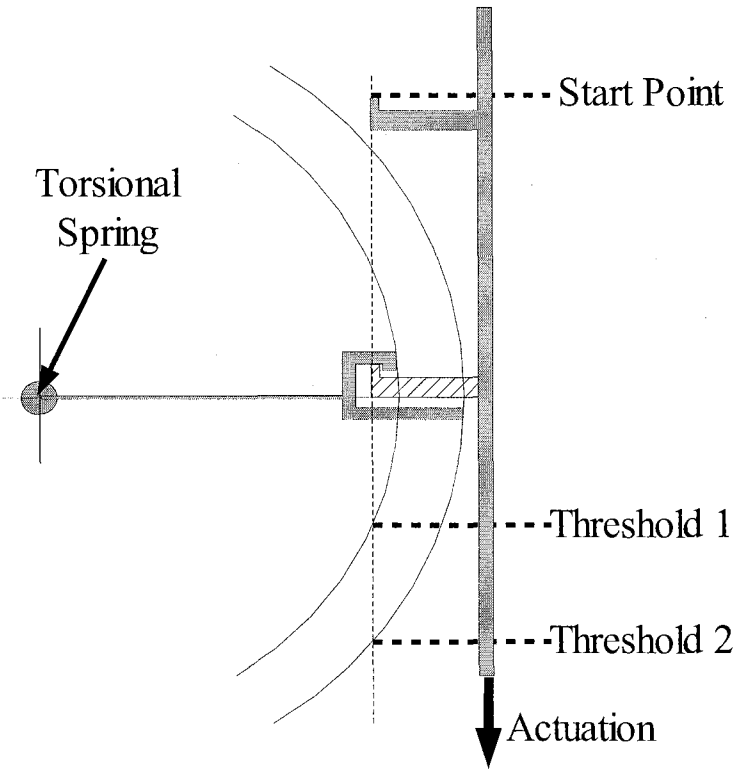

Figure 3.10: Compliant Extension Ladder Based Bistable Mechanism

The thresholds depicted in Figure 3.10 lie at the intersection of the line that traces the movement of the leftmost edge of the rung and the arcs that trace the motion of the two rightmost points of the hook. These thresholds function the same way as for the

design with a rotational joint. Normal operation of the compliant extension ladder based bistable mechanism is depicted in Figure 3.11.

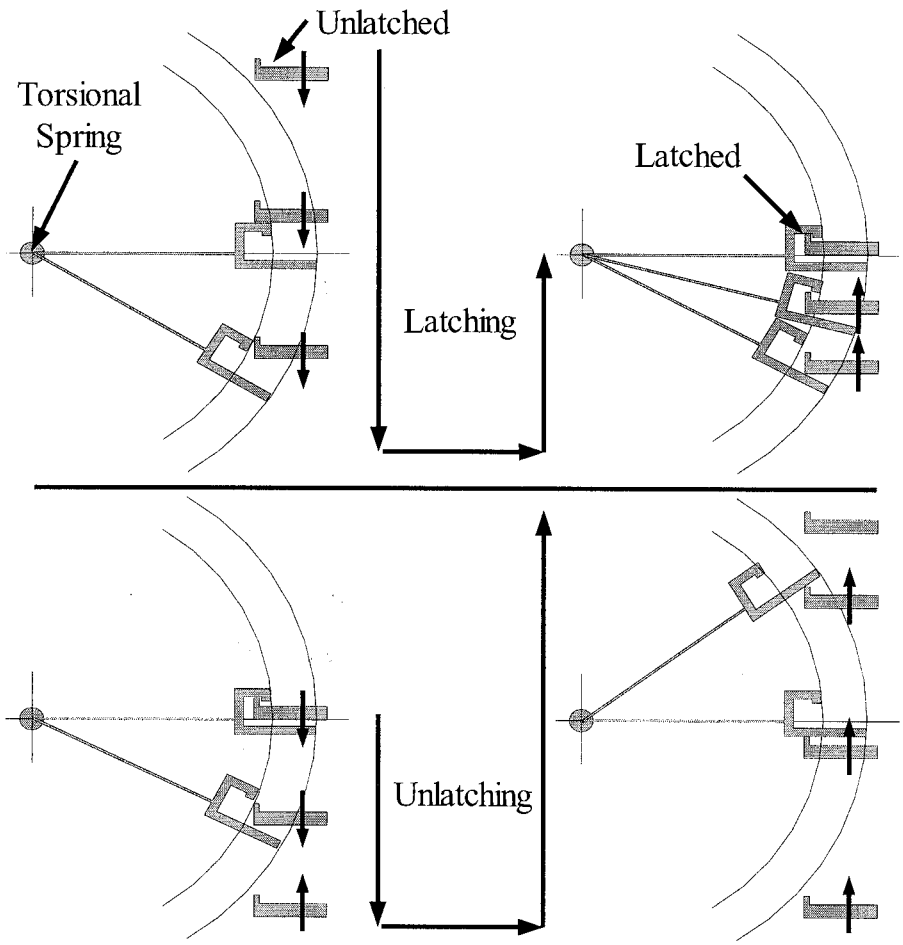

Figure 3.11: Latching and Unlatching Motion of the Compliant Extension Ladder Bistable Mechanism

The complaint version of the extension ladder bistable mechanism is ongoing work of the author. However, the extension ladder bistable mechanism was unable to fulfil the original intent of creating a single digital input bistable mechanism.

3.2.2 Magnetic Bistable Mechanism

The magnetic bistable mechanism designed by M. Ruan, et al. [23] uses a combination of soft and hard magnetic materials to achieve bistable functionality. Figure 3.12 illustrates the design of the magnetic bistable mechanism.

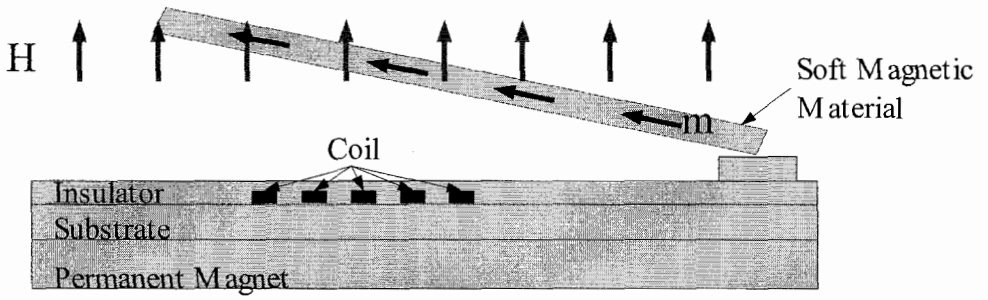

Figure 3.12: Schematic of Magnetic Bistable Mechanism [xix]

The soft magnetic material used in this design was a NiFe permalloy. A planar coil is used to actuate the cantilever between stable states. This design operates on the principle that the soft magnetic cantilever will try to align itself with the magnetic field. Figure 3.13 describes how this tendency of the cantilever to align itself to the permanent magnetic field is used to achieve two separate torques.

[xix] Figure by author, based on the cited work.

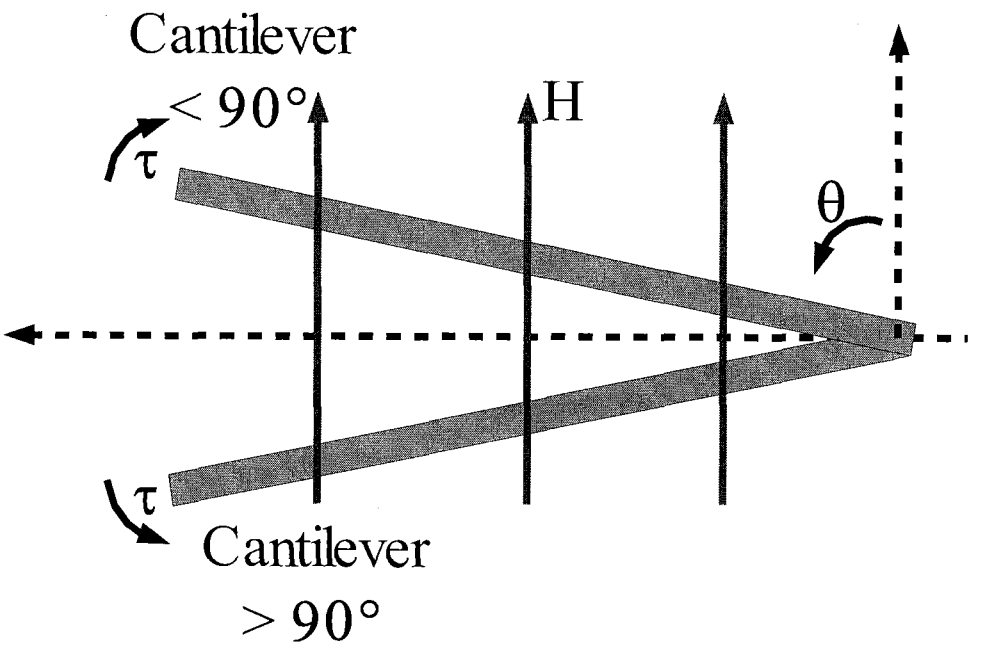

Figure 3.13: Operating Principle of Magnetic Bistable Mechanism

The soft magnetic cantilever will try to align itself to the permanent magnetic field by rotating the shortest angular distance. When θ is less than 90°, the cantilever undergoes a clockwise torque to bring it in line with the permanent field. A clockwise torque pushes the cantilever away from the surface of the substrate, opening an electrical circuit, which results in an off state. When θ is greater than 90°, the cantilever undergoes a counter-clockwise torque to bring it in line with the permanent field. A counter-clockwise torque pushes the cantilever towards the surface of the substrate, completing an electrical connection. Because the alignment is to a permanent magnetic field, each of these two states is stable. To switch between the two states the coil is energized with a pulse of current causing the magnetic field to momentarily switch directions.

The magnetic mechanism has the advantage of only requiring one input to operate, however, the disadvantages are that: the input is analog, the device utilises a non-standard fabrication process and the footprint of this device is 1000μm x 600 μm.

3.2.3 Liquid Metal Electrostatic Switch

L. Latorre, et al. designed the liquid metal electrostatic switch [21] consisting of a droplet of mercury that is electrostatically actuated to complete an electrical circuit. The schematic for the liquid metal electrostatic switch is given in Figure 3.14.

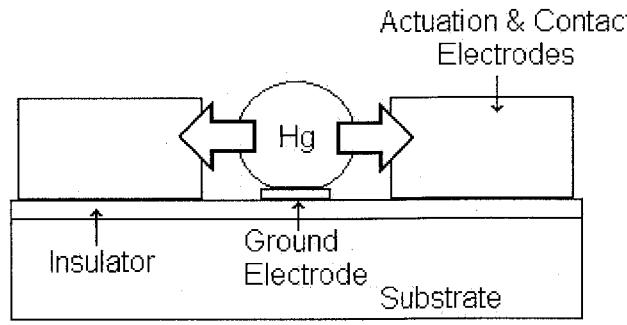

Figure 3.14: Liquid Metal Electrostatic Switch [xx]

This switch is operated by applying a large voltage between one of the contact electrodes and the ground electrode. Electrostatic attraction then causes the mercury droplet to move until it completes the circuit between the contact and ground electrodes, where it stays in position because of surface tension.

Although this switch is simple and can be made quite small, it requires voltages that range from 100 to 400 volts to actuate the liquid metal droplet. As well, this switch

[xx] Figure by author, based on the cited work.

is limited in application to relays as the output is electrical only and cannot be mechanically coupled to other mechanisms.

3.3 Performance Measures

I propose two different performance measures of bistable mechanisms beyond basic bistable functionality. They are the ratio of displacement to actuation and the ratio of displacement to area. These measures of performance will be used as objective criteria for the evaluation of the presented designs.

3.3.1 Displacement/Actuation Ratio

The displacement/actuation ratio is a measure of the distance between the two stable states normalized to the distance that the device must be actuated to switch states. This measure is unitless and scaling independent, meaning for a given device, this measure stays constant as the device is scaled for different applications. Figure 3.15 illustrates the displacement/actuation ratio using the extension ladder based bistable mechanism that was described in section 3.2.1.2.

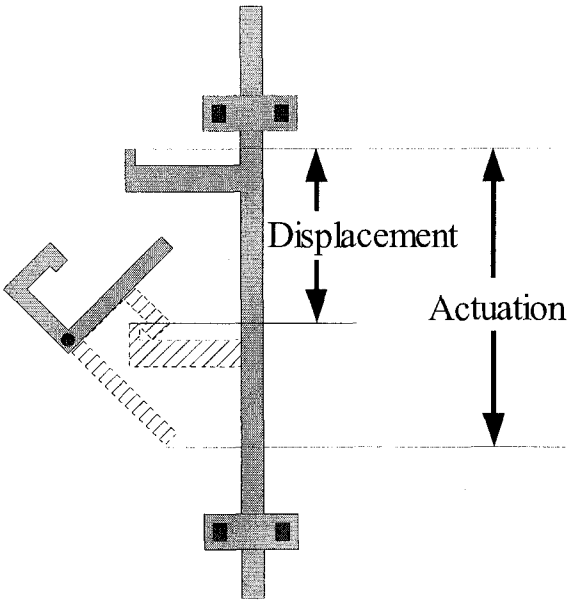

Figure 3.15: Illustration of the Displacement/Actuation Ratio

The purpose of this performance measure is to provide a measure of the overshoot required when switching states. This measure also gives an indication of what kind of actuation method will be needed for a given displacement.

3.3.2 Displacement/Area Ratio

The displacement/area ratio is a measure of the distance between the two stable states normalized to the area that the device takes up on the substrate. This measure has the units of m^{-1} and is scaling dependent. As a result, this measure will degrade as a device is scaled larger and should only be used to evaluate designs that provide the same displacement. Figure 3.16 illustrates the displacement/area ratio using the extension ladder based bistable mechanism.

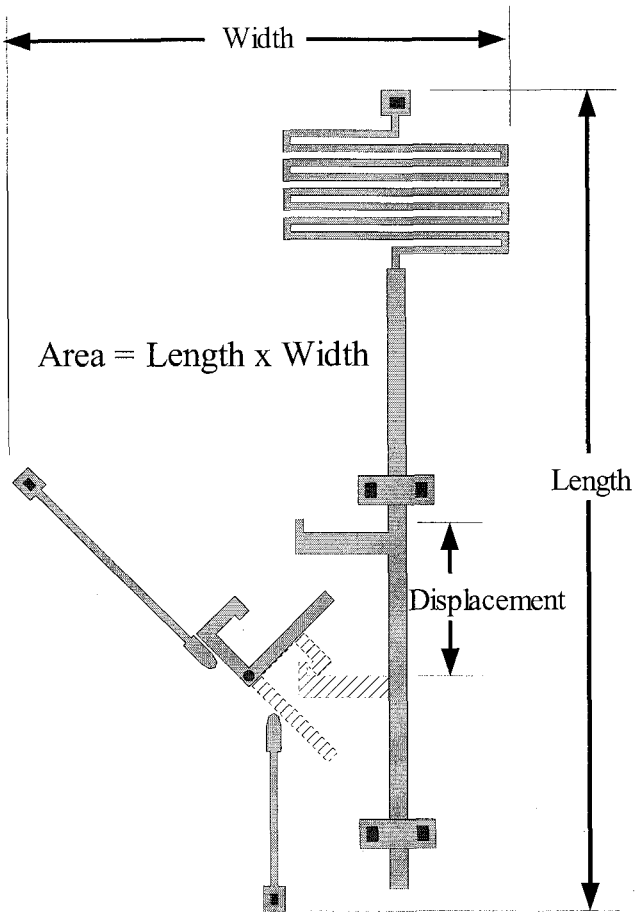

Figure 3.16: Illustration of the Displacement/Area Ratio

The goal of a bistable mechanism is to provide a physical displacement between stable states. This measure gives an indication of how efficiently a design meets this goal with respect to the design area used. A design that can accomplish the same goal and uses less area will be less expensive to produce. Table 3.1 summarizes the various bistable mechanisms and some of their properties.

3.4 Current Bistable Mechanisms Summary

Table 3.1: Summary of Bistable Mechanisms in the MEMS Literature

Design	Footprint (μm)	Inputs	In Plane	Standard Fabrication Process Compatible	Displacement Actuation Ratio	Displacement Area Ratio (×1000)
Classic Compliance(3.1.1)	243 x 140	2 Digital	Yes	Yes	1	0.41
Centrally Clamped Beam(3.1.2)	3000 x 480	2 Digital	Yes	Yes	1	0.33
Snapping Actuator(3.1.3)	200 x 70	3 Digital	No	No	1	0.86
Young Mechanism(3.1.4)	300 x 200	2 Digital	Yes	Yes	1	1.6
Multimorph Cantilever(3.2.1.1)	860 x 100	2 Digital	No	No	0.75	0.38
Extension Ladder (3.2.1.2)	330 x 640	1 Analog	Yes	Yes	0.75	1.4
Magnetic(3.2.2)	1000 x 600	1 Analog	No	No	1	0.0033
Liquid Metal(3.2.3)	60 x 60	2 Analog	Yes	No	1	5.5

4 THE HYSTERESIS SPRING BISTABLE MECHANISM

The hysteresis spring bistable mechanism utilizes the clamping and unclamping of a spring's anchor to introduce hysteresis to the movement of a latch. The hysteresis spring allows for the creation of a bistable mechanism that has a single digital input. In order to understand the function of the hysteresis spring bistable mechanism, a description of the hysteresis spring will be given first followed by a functional description of the entire device. An analytical model of the hysteresis spring bistable mechanism will be developed in order to more fully understand the effect of the various design parameters. Modelling will also be approached using the finite element method and the results presented. Devices fabricated using the PolyMUMPS technology were tested and the results will be discussed. To complete the discussion of the hysteresis spring bistable mechanism, the models and fabrication results will be compared.

4.1 The Hysteresis Spring Element

The hysteresis spring is a regular spring, which has a switchable ground instead of being directly anchored to ground. Figure 4.1 shows a simple hysteresis spring.

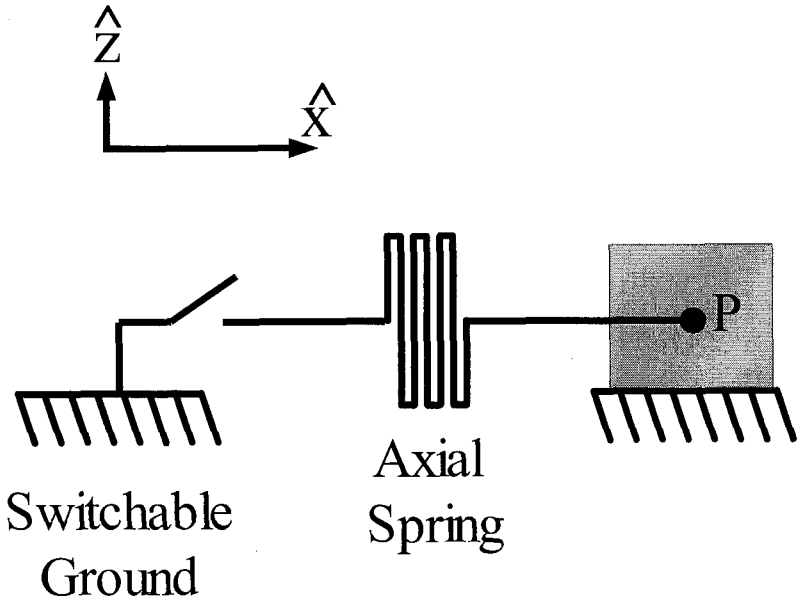

Figure 4.1: Simple Hysteresis Spring

To illustrate the operation of a hysteresis spring, consider the force exerted by the spring on the point P in the following scenario. An actuator attached to point p has a force displacement relationship as follows:

$$F_x = k_s(2 - x) \qquad \textbf{Equation 4.1}$$

Where k_s is the spring constant of the hysteresis spring. If the ground for the spring and the actuator are turned on then point P will move in the X direction and settle in a new equilibrium position (X = 1) where the force from the actuator and spring balance. If point P is then latched into this new equilibrium position and the actuator and spring ground are turned off, then the spring will relax and no force will exist in either direction on P. Now, if the spring ground and actuator are turned back on, P will reach a

new equilibrium point at X = 1.5. Figure 4.2 shows a graphical representation of how the two equilibrium points are reached in this example.

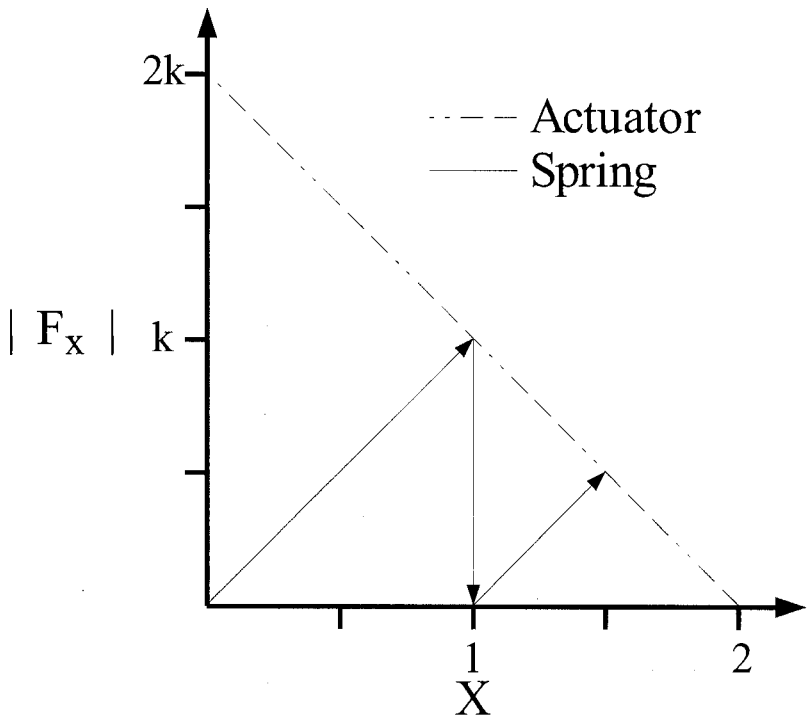

Figure 4.2: Hysteresis Spring Example

The hysteresis spring has in this example succeeded in creating hysteresis in the movement of point P. When the actuator and ground are both engaged the resulting equilibrium point is dependent on the previous state of the device, and thus memory has been introduced into this system

The hysteresis spring requires two items to operate in the manner required for a single digital input bistable mechanism; a switchable ground and some form of latch to hold the output in the equilibrium position. If, no switchable ground exists, the output point P will always follow the same path for a given actuation, making the goal of producing a single digital input bistable mechanism impossible. A latch to hold the

output in the equilibrium position is required because, without some form of latch to hold the output point's position, when the actuation is removed the mechanism will return to its original or fabrication state. The memory retention property of the hysteresis spring will be rendered useless if the mechanism is always being actuated from the same position, as the state being remembered will never change.

The hysteresis spring utilized in the bistable mechanism design is acting in-plane and is creating hysteresis in a two dimensional movement. Taking the two dimensional movement into account requires a more complex model than that of a single axial spring, because the spring used will undergo both compression and torque. To deal with these two different effects, modelling the spring as two different springs, one axial spring and one torsional spring, is beneficial. Figure 4.3 shows the model of the hysteresis spring acting in two dimensions.

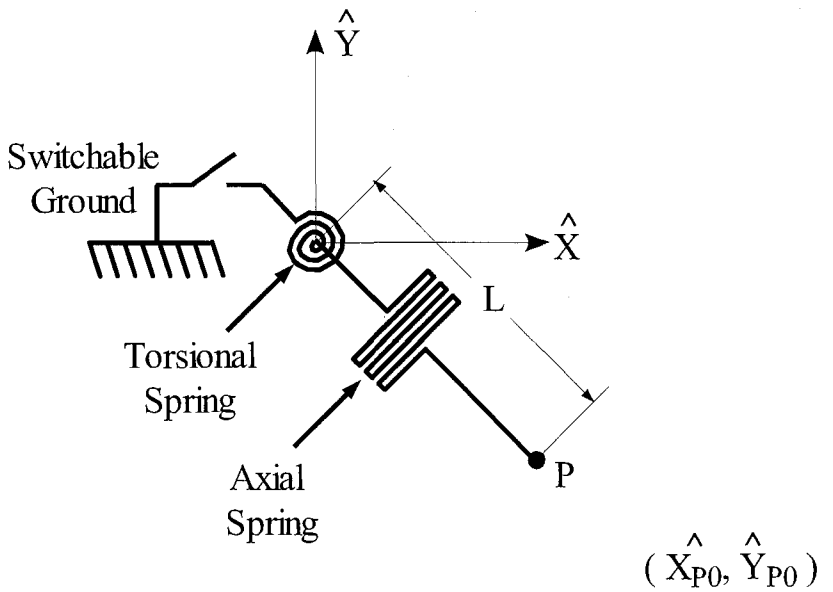

Figure 4.3: Model of Hysteresis Spring Acting in Two Dimensions

The model of the hysteresis spring is discussed in detail in section 4.3.

4.2 Functional Description

The hysteresis spring bistable mechanism utilizes the clamping and unclamping of a spring's anchor to introduce hysteresis to the movement of a latch. The hysteresis spring bistable mechanism has two stable positions: the unlatched (as fabricated) position and the latched position.

The most simplified version of the hysteresis spring ignores the affect of rotation on the performance of the hysteresis spring. This simplification allows for a more intuitive understanding of the operation of the hysteresis spring bistable mechanism. The basic layout of a hysteresis spring bistable mechanism and the corresponding simple model is given in Figure 4.4.

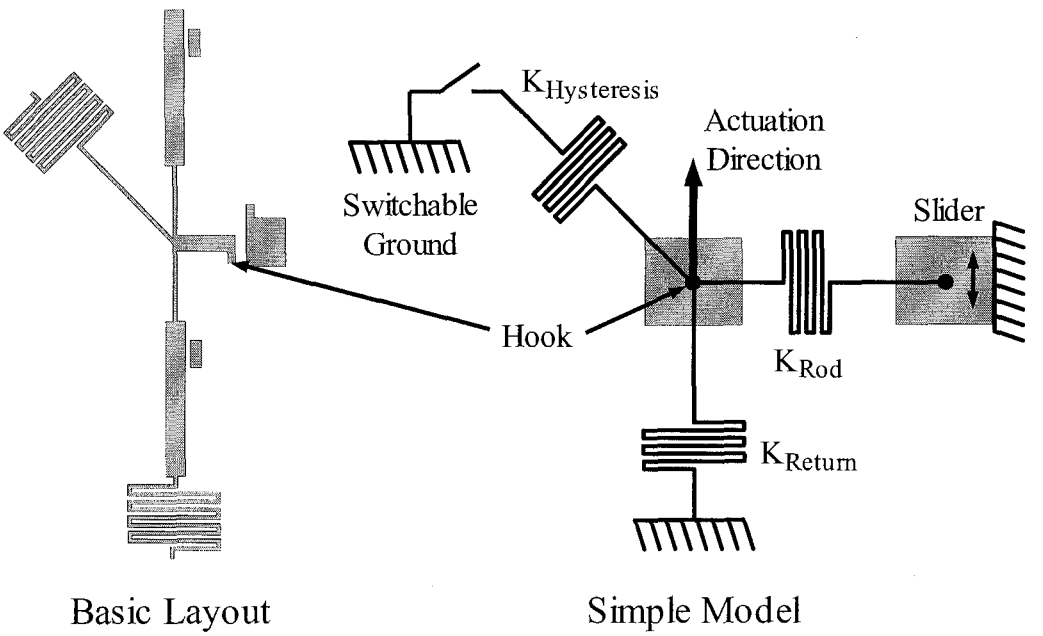

Figure 4.4: Basic Layout and Simple Model of the Hysteresis Spring Bistable Mechanism

In a transition from unlatched to latched states, the hysteresis spring is anchored by the switchable ground, causing lateral movement and the hook to latch. When transitioning from latched to unlatched states, the hysteresis spring is allowed to relax which results in a lesser lateral force when it is again engaged. This allowed the hook to miss the catch. Figure 4.5 shows a simplified set of the forces acting on the hook as it reaches a displacement near the latched state.

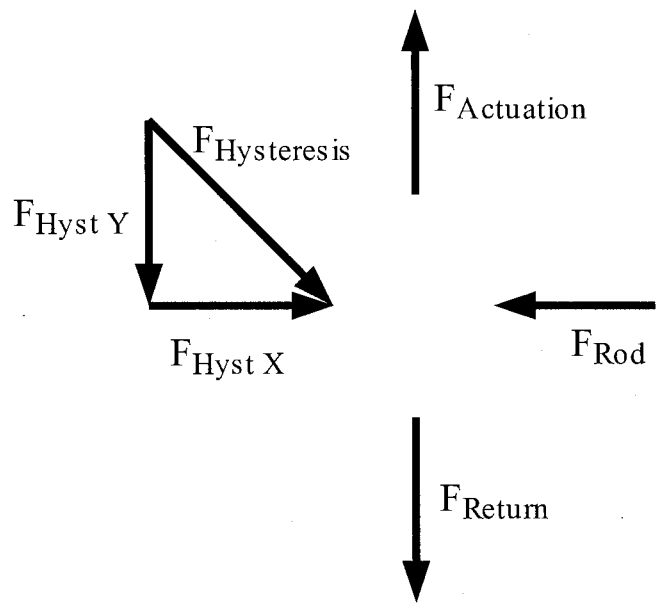

Figure 4.5: Simplified Force Diagram for State Transition.

Based on these forces, three conditions must be satisfied for the state transition's successful completion. The first condition is the actuation condition given in Equation 4.2.

$$F_{Actuation} > F_{HystY} + F_{Return} \qquad \textbf{Equation 4.2 Actuation Condition}$$

This condition indicates that the actuation force must be capable of overcoming the spring forces so that it can move the hook up to the catch.

The second condition is the latching condition, which is required for a successful transition from unlatched to latched states.

$$F_{HystX} > F_{Rod}$$ **Equation 4.3 Latching Condition**

This condition indicates that the force of the hysteresis spring must be greater than the spring force created by the deformation of the rod in order to allow the hook to move to the right and latch.

The third condition is the unlatching condition, which is required for a successful transition from latched to unlatched states.

$$F_{HystX} < F_{RodX}$$ **Equation 4.4 Unlatching Condition**

This condition indicates that the force of the hysteresis spring must be less than the spring force created by the deformation of the rod. This condition allows the hook to move to the left and unlatch.

Clearly, based on these conditions, memory must exist in the system so that, depending on the current state, a larger or smaller lateral force is provided. This memory is provided through the use of the hysteresis spring.

The movement of the hook during the latching and unlatching movements is shown in Figure 4.6.

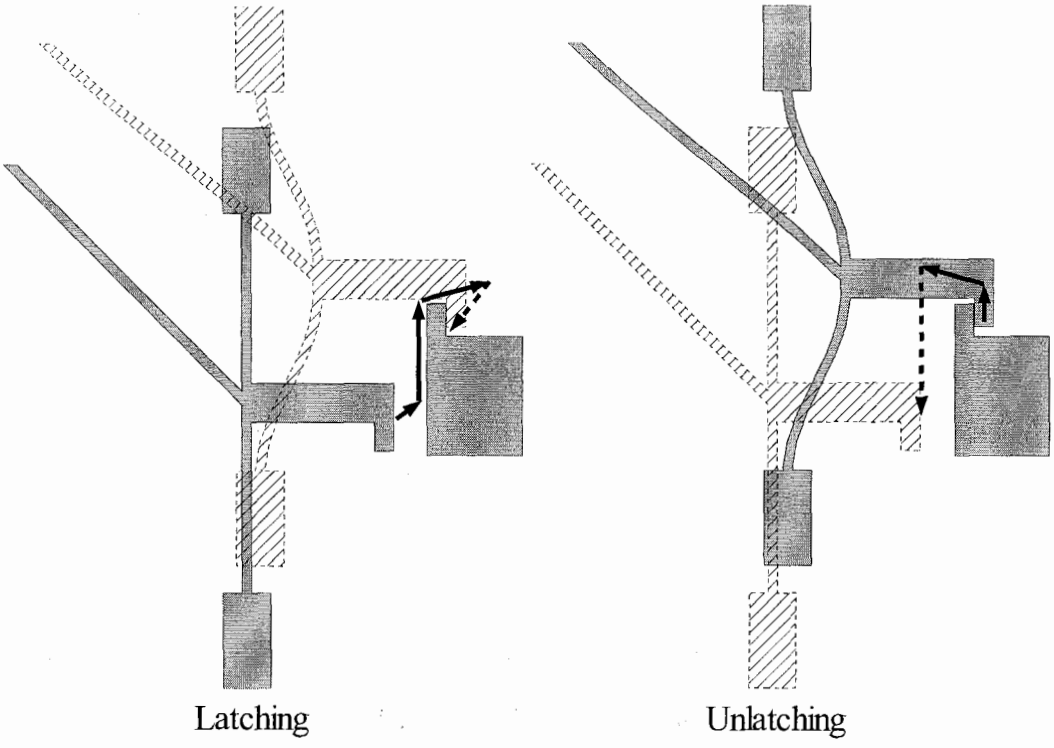

Figure 4.6: Latching and Unlatching of the Hook and Catch

In Figure 4.6, the solid arrows show the movement of the hook when power is applied, whereas the dotted arrows show the movement of the hook once power has been removed.

Two separate actuators are required to operate the mechanism: one to clamp the spring, creating the switchable ground and one to pull the rod in the Y-direction, bringing the hook up to the level of the catch. For the mechanism to latch, the hysteresis spring must be engaged for enough of the Y-direction travel to provide sufficient lateral force to allow latching. If this device were operated using two inputs, the clamp would first be engaged and then the mechanism would be actuated in the Y-direction. Sequential actuation ensures that the lateral force provided by the hysteresis spring would be maximized, as the lateral force is proportional to the movement in the Y-direction.

However the purpose of this thesis is to develop a single digital input bistable mechanism. To achieve this purpose the two actuators must be connected to the same digital input signal and be actuated simultaneously. For simultaneous actuation to operate the device correctly, the clamp has to engage before the Y-direction actuation reaches its maximum value so that the hysteresis spring provides lateral force. The solution is to have the clamp actuator engage the clamp well before the actuator has reached full deflection. For example, if a thermal actuator having a maximum deflection of 8μm at 5 volts was used for the clamping mechanism, the clamp should be designed to engage at a small deflection such as 2μm. This design would allow the hysteresis spring to be engaged for 75% of the actuation in the Y-direction.

The actuations are performed through directly coupled actuators. The fabricated design uses probes to provide the actuation, however, the function of the hysteresis spring bistable mechanism is independent of the actuation method. Any actuator that can provide the required actuation characteristics can be utilized.

4.3 Analytical Model

The purpose of the analytical model is to provide a tool for basic design. The model should be able to predict the equilibrium displacement of the hook in the X-direction for a given Y displacement and set of design parameters. This model will allow the designer to determine the range of design parameters that are able to achieve their goal of a bistable mechanism meeting a state displacement criterion. For example, the proof of concept designs required an X displacement of 6μm at a Y displacement of 25μm to allow for latching. The model can be used to predict the design parameters required to provide 6μm of X displacement for the given Y displacement.

4.3.1 A Simple Model

The initial analytical model considered did not take rotational effects into account. The simple model used is depicted in Figure 4.7.

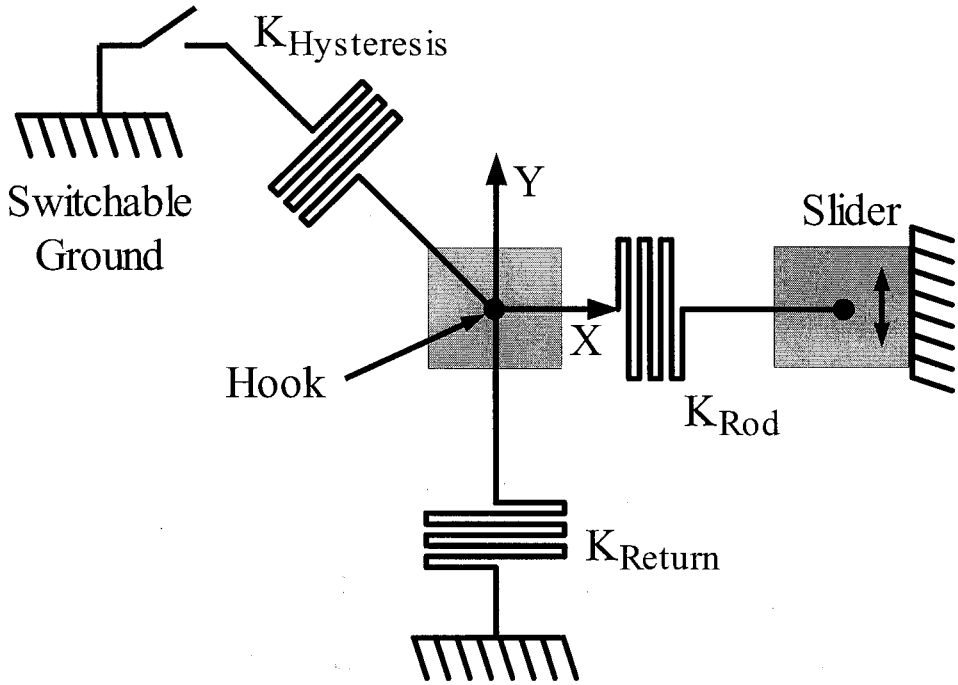

Figure 4.7: Simple Model of Hysteresis Spring Design

The goal of the modelling of this device is to find the motion of the tip of the hook in the X direction as a function of the motion in the Y direction as well as the various spring constants. Knowing the motion of the tip of the hook allows for correct placement of the catch.

As stated, this simple model does not take rotation into account, resulting in the assumption that the hysteresis spring is at 45° throughout operation. This assumption leads to Equation 4.5.

$$f_{HystY} = -K_{Hyst}\, y \qquad \textbf{Equation 4.5}$$

The force the in the Y-direction is directly proportional to the hysteresis spring constant in a negative direction. Also following from the 45° assumption is Equation 4.6.

$$f_{HystX} = -f_{HystY}$$ **Equation 4.6**

Equation 4.6 states that force produced by the hysteresis spring in the X-direction is equal in magnitude to the force produced in the Y-direction. The other force acting in the X-direction comes from the deformation of the rod. Equation 4.7 gives the relationship for the force produced in the X-direction by the deformation of the rod.

$$f_{Rod} = -K_{Rod}\, x$$ **Equation 4.7**

The equilibrium X position of the hook is determined whenever the summation of the forces in the X-direction is zero. This equilibrium position is described in Equation 4.8.

$$f_{Rod} + f_{HystX} = 0$$ **Equation 4.8**

If Equation 4.6 and Equation 4.7 are combined with Equation 4.8 and rearranged, the result is the relationship between the X and Y displacements. Equation 4.9 describes the motion of the tip of the hook in the X direction as a function of the motion in the Y direction and the various spring constants.

$$X = \frac{K_{Hyst}\, y}{K_{Rod}}$$ **Equation 4.9**

This simple model, while useful for determining order of magnitude values for displacement and force, does not provide values that match with finite element modelling or the fabricated devices (Section 5.2). These discrepancies are due to the assumptions made in the generation of the simple model. As a result, a second model was developed that included rotational motion.

4.3.2 Rotational Model

Because the simple model was found not to agree with the Finite Element Analysis and fabricated results, the rotational model was developed to correct the deficiencies. The rotational model represents the hysteresis spring as a combination of a rotational spring and separate axial spring rather than just a simple axial spring. Figure 4.8 depicts the rotational model with some of the variables used in the analysis.

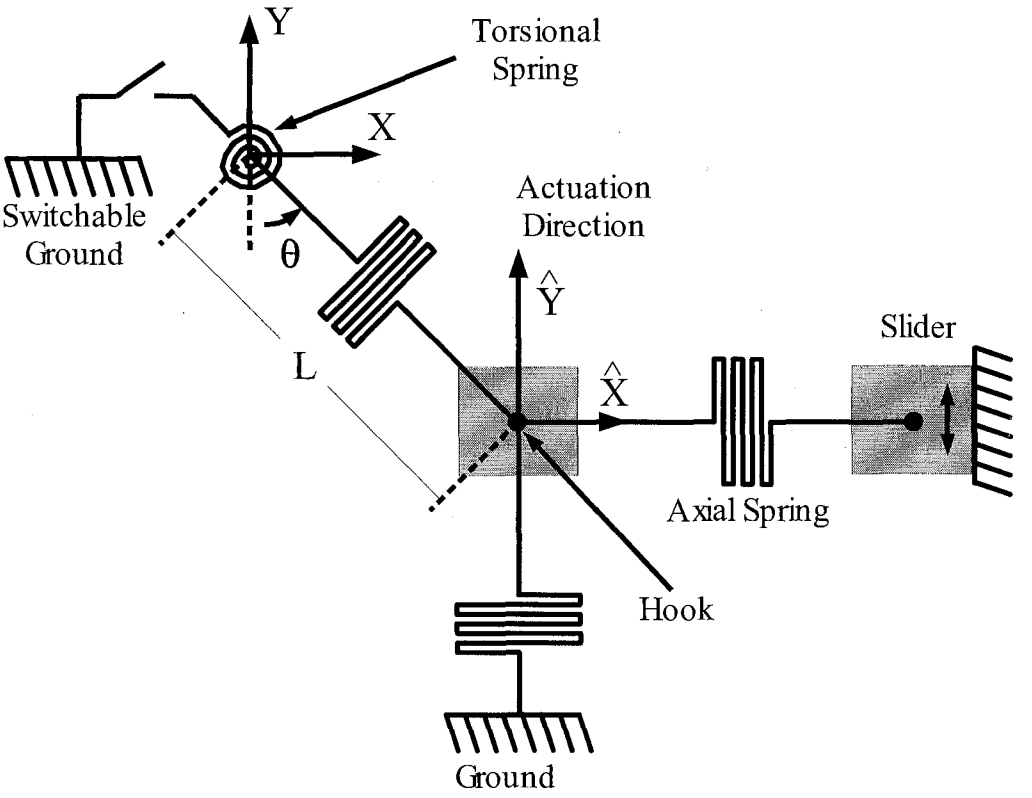

Figure 4.8: Rotational Model for the Hysteresis Spring Bistable Mechanism

The first set of forces considered in the analysis are the forces relating to the hysteresis spring. Because the hysteresis spring has been modelled as separate axial and torsional springs, the forces in the axial and the tangential directions are determined in

terms of the variables that describe the hysteresis spring. Equation 4.10 gives the relationship between the spring's axial force and the spring's change in length.

$$f_{HystAxial} = (L - r)\, K_{HystAxial} \qquad \textbf{Equation 4.10}$$

Where: L is the initial rest length of the hysteresis spring from the center of rotation to the attachment point with the hook; r is the variable length of the hysteresis spring from the center of rotation to the attachment point with the hook; and $K_{HystAxial}$ is the spring constant of the axial portion of the hysteresis spring.

Equation 4.11 gives relationship between the spring's tangential force and the torque generated by the torsional spring.

$$f_{HystRotational} = \frac{\tau}{r} \qquad \textbf{Equation 4.11}$$

Where: τ is the torque generated by torsional spring; and r is as defined in Equation 4.10.

The torque is proportional to the angular change of the hysteresis spring as described in Equation 4.12.

$$\tau = \beta_{HystRotational} (\theta - \theta_0) \qquad \textbf{Equation 4.12}$$

Where: β is the torsional spring constant; θ is the angle between the negative Y-axis and the axis of the hysteresis spring; and θ_0 is the initial value of θ (45°).

Equation 4.10 and Equation 4.11 give the axial and tangential force relationships in polar coordinates. The final solution should be in rectangular coordinates form, therefore, Equation 4.13 and Equation 4.14 express the components of the axial and tangential forces in the X and Y directions respectively.

$$f_{HystX} = \sin(\theta) f_{HystAxial} - \cos(\theta) f_{HystRotational}$$ **Equation 4.13**

$$f_{HystY} = -\cos(\theta) f_{HystAxial} - \sin(\theta) f_{HystRotational}$$ **Equation 4.14**

The next set of forces described are those that are the result of the other springs in the model. Equation 4.15 describes the force displacement relationship that results from the deformation of the rod.

$$f_{Rod} = -K_{Rod} X_{hat}$$ **Equation 4.15**

Where: K_{Rod} is the spring constant of the deformable portion of the rod; and X_{hat} is the displacement of the hook in the X-direction referenced from the as fabricated rest position of the hook.

Equation 4.16 describes the force displacement relationship for the returning spring.

$$f_{Return} = -K_{Return} Y_{hat}$$ **Equation 4.16**

Where: K_{Return} is the spring constant of the returning spring; and Y_{hat} is the displacement of the hook in the Y-direction referenced from the as-fabricated rest position of the hook.

The equilibrium X position of the hook is reached whenever the summation of the forces in the X-direction is zero. This equilibrium is described in Equation 4.17.

$$f_{Rod} + f_{HystX} = 0$$ **Equation 4.17**

When Equation 4.13 and Equation 4.15 are substituted into Equation 4.17, the resulting equation has five variables as shown in Equation 4.18:X, Y, X_{hat}, θ and r.

$$f_{Xdir} = \sin(\theta)\,(L - r)\,K_{HystAxial} - \frac{\cos(\theta)\,\beta_{HystRotational}\left(\theta - \frac{\pi}{4}\right)}{r} - K_{Rod}X_{hat} \qquad \textbf{Equation 4.18}$$

However, X_{hat}, θ and r are determined as functions of X and Y. Equation 4.19 through Equation 4.21 describes X_{hat}, θ and r in terms of X and Y respectively.

$$X_{hat} = x - \frac{L}{\sqrt{2}} \qquad \textbf{Equation 4.19}$$

$$\theta = \arctan\left(-\frac{x}{y}\right) \qquad \textbf{Equation 4.20}$$

$$r = \sqrt{y^2 + x^2} \qquad \textbf{Equation 4.21}$$

When Equation 4.19 through Equation 4.21 are substituted into Equation 4.18, the force in the X-direction is expressed as a function of X and Y as well as the physical constants of the system, as shown in Equation 4.22.

$$f_{Xdir} = -\frac{x\left(L - \sqrt{y^2 + x^2}\right)K_{HystAxial}}{\sqrt{y^2 + x^2}} - \frac{y\,\beta_{HystRotational}\left(-\arctan\left(\frac{x}{y}\right) - \frac{\pi}{4}\right)}{y^2 + x^2} - K_{Rod}\left(x - \frac{L}{\sqrt{2}}\right) \qquad \textbf{Equation 4.22}$$

Because only the equilibrium X displacement is of interest, the solutions to consider are those that yield $F_{Xdir} = 0$.

4.3.2.1 Parameter Plots

In the equation resulting from $F_{Xdir} = 0$, analytically isolating the X variable and considering the affects of the various design parameters on the X displacement, is difficult. As a result, plots utilizing numerical methods were made around a center design at three different Y displacements. These plots are intended to show the affect of

each design parameter on the X displacement, so that a designer can predict which design parameters should be changed to provide a desired change in X displacement. The values of the various design parameters for this center design are summarized in Table 4.1.

Table 4.1: Design Parameters For Center Design

Design Parameter	Center Value
$\beta_{HystRotational}$	1.11267×10^{-9} N·m·rad^{-1}
$K_{HystAxial}$	4.79846 N·m^{-1}
K_{Rod}	1.80267 N·m^{-1}
L	150 μm

The X displacement as a function of Y displacement is nearly linear around the center value. A numerical plot of this relationship is illustrated in Figure 4.9.

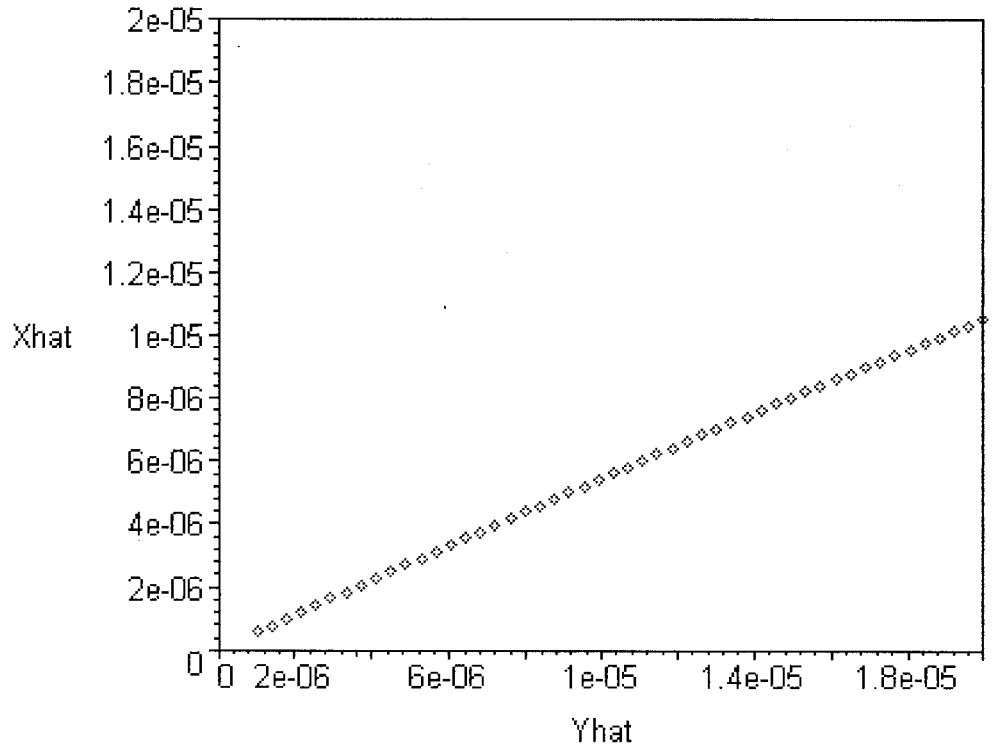

Figure 4.9: Plot of $X_{hat} \propto Y_{hat}$ Relationship Around the Center Design Value

From Figure 4.9, the expected motion of the unimpeded hook is linear with respect to Y displacement.

Varying the design parameters changes the slope of the $X_{hat} \propto Y_{hat}$ relationship. In order to see the trends around the center design, Figure 4.10 through Figure 4.13 show plots of the X_{Hat} displacement versus design parameter values around the center design.

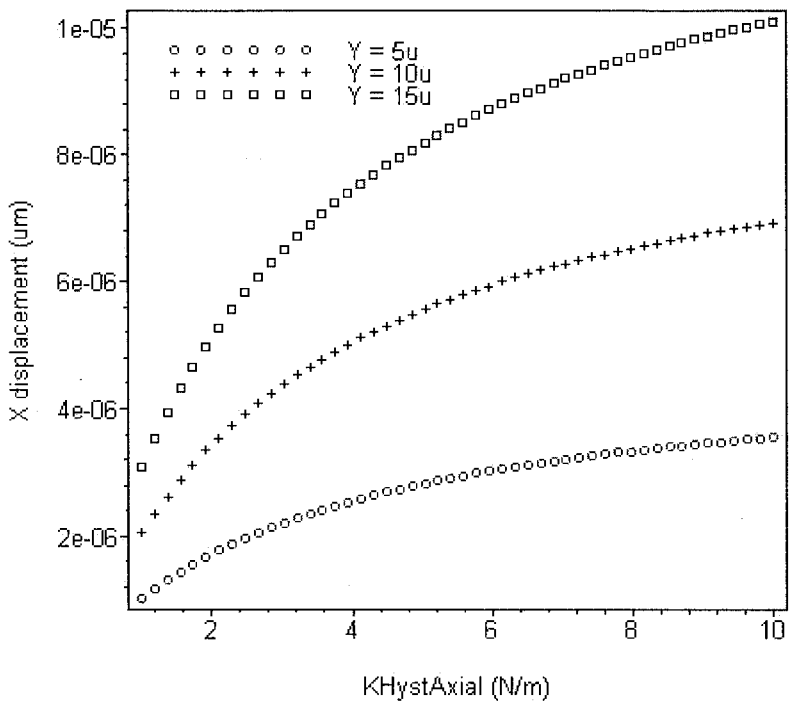

Figure 4.10: Plot of $X_{hat} \propto K_{HystAxial}$ Relationship Around the Center Design Value

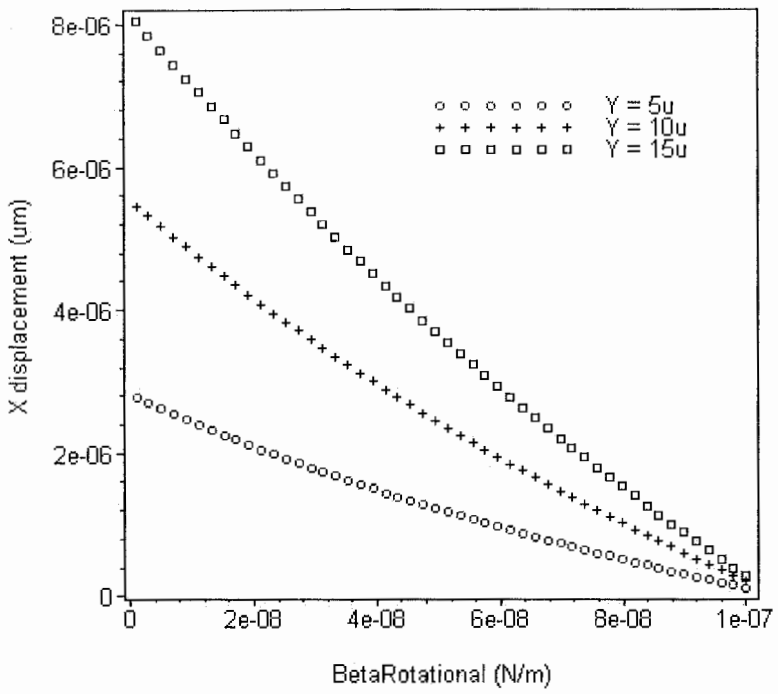

Figure 4.11: Plot of $X_{hat} \propto \beta_{HystRotational}$ Relationship Around the Center Design Value

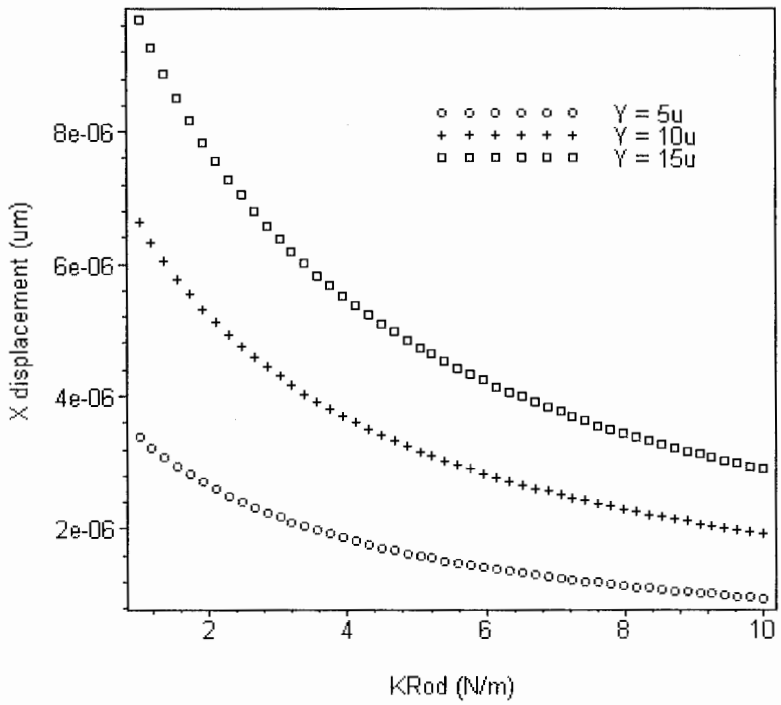

Figure 4.12: Plot of $X_{hat} \propto K_{Rod}$ Relationship Around the Center Design Value

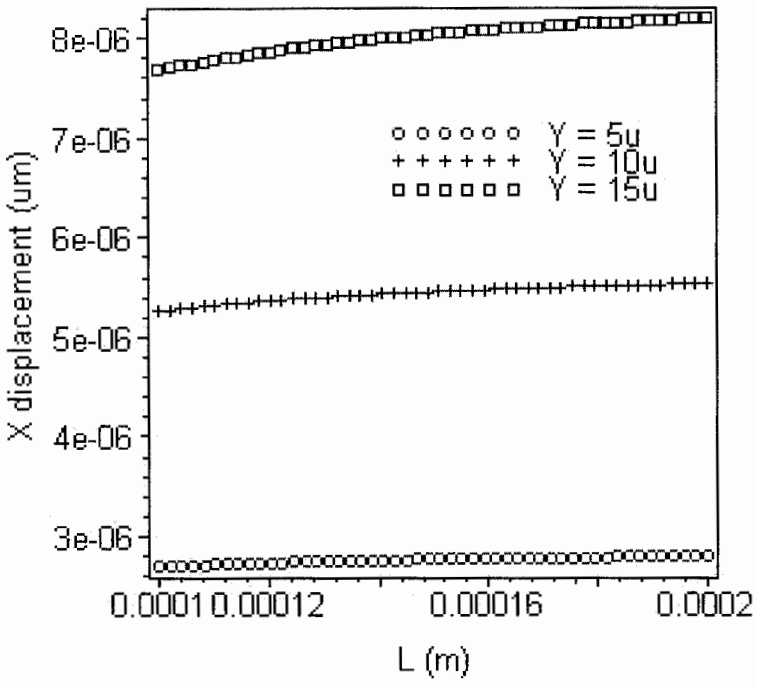

Figure 4.13: Plot of $X_{hat} \propto L$ Relationship Around the Center Design Value

The center design was chosen to provide an X displacement that is approximately half the Y displacement. The slope of the X versus Y displacement relationship is changeable using the gradient information in these graphs to determine which design parameters should be changed and in which direction they should be changed. Alternatively, design optimization is accomplished numerically using a cost functional. This problem of optimal design is an area into which further work could be undertaken.

4.4 Finite Element Model

Finite Element Analysis, or FEA, is a numerical technique for finding the response of a device to stimulus. FEA takes a complex geometry for which an analytical solution is difficult to find or does not exist and approximates the geometry with small segments called elements. In the two dimensional case, these elements are triangles or

quadrilaterals, which are easily solvable. The stimulus is then applied to the approximated geometry and the phenomenon of interest is calculated over the simple elements.

FEA is most useful for cases where a closed form solution is not easily determined. While an approximate closed form solution to the movement of the hysteresis spring bistable mechanism is attainable by simplification of the model (see section 4.3), a true closed form expression cannot be easily found because all portions of the switch are compliant, not just the portions designed as springs. The inability to determine a complete closed form expression makes the hysteresis spring bistable mechanism a good candidate for FEA.

4.4.1 Geometric Model

To generate the geometric model for analysis, the design layouts were converted to the ANSYS Neutral Format (.ANF). In order to simplify the analysis, the structure was altered to be two-dimensional and the pad and the ring that are used to actuate the mechanism were removed. This simplification was performed before the layout conversion. One of the layouts used for the hysteresis spring bistable mechanism is shown in Figure 4.14 before any modifications were undertaken.

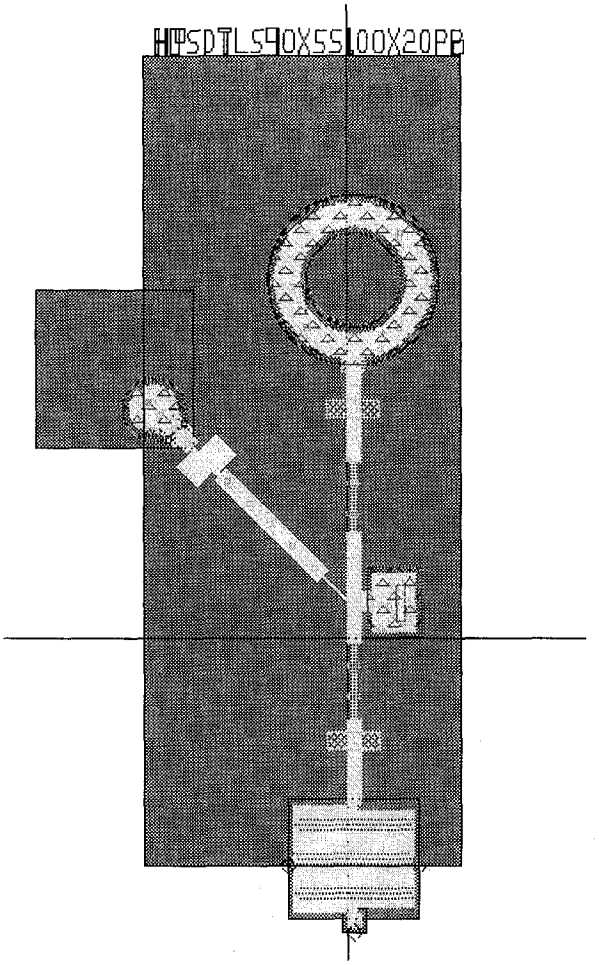

Figure 4.14: Hysteresis Spring Bistable Mechanism Layout

In the conversion to two dimensions, only the POLY1 layer of the design was converted because it contains the relevant structures of the design. The rest of the layers contain connections to the substrate that anchor portions of the device and staples to constrain vertical movement of the device. All of these structural functions, lost in the conversion, can be modelled using boundary conditions.

The removal of the pad and ring require the assumption that they can be modelled using boundary conditions. In this design, the pad and ring are present only to introduce displacement boundary conditions on the ends of the two rods and can be replaced by any

actuators that produce the same displacement boundary conditions. Therefore, the pad and ring are good candidates to be removed and replaced with just boundary conditions.

Software developed by Robert (Bobby) Johnstone was used to perform the layout conversion. This software is web accessible at the following website: http://www.sfu.ca/~rjohnsto/layout2layout.html. The "layout2layout" software performs a raw conversion of one layout format to another. This software saves a considerable amount of work by removing the need to redefine the geometries using ANSYS' preprocessor.

Figure 4.15 shows the final ANSYS model geometry for the hysteresis spring design shown in Figure 4.14.

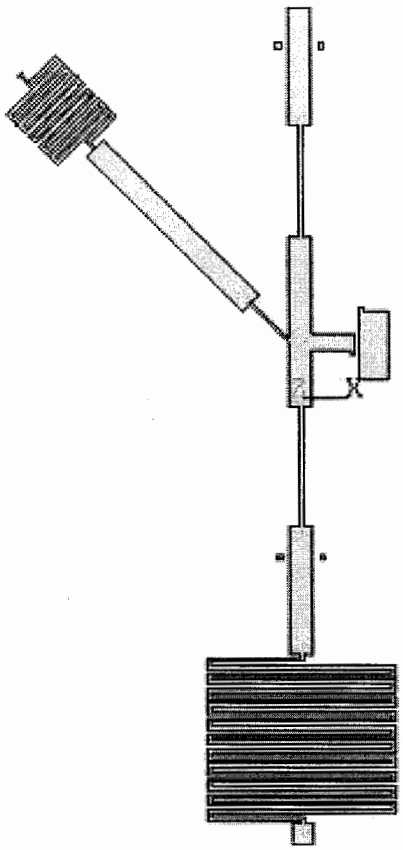

Figure 4.15: ANSYS Model of the Hysteresis Spring Bistable Mechanism

4.4.2 Assumptions

The geometric simplifications made in the conversion of the layout to an ANSYS friendly format are only a part of the simplifications made in the analysis. Further assumptions were made and used to simplify the analysis of the finite element model. These assumptions are summarized in

Table 4.2:Assumptions of FEA Simplification

Assumptions	Reality
Interactions only in-plane	Out-of-plane buckling can occur
Actuator pulls in only the Y-direction	An actuator pair could pull in only the Y-direction but using a wafer probe to pull the ring will cause some movement in the X and Z-directions.
Anchors are stationary and act only in-plane	Anchors will apply some out-of-plane torque to the structure.
Staples constrain non-spring portion of rod to movement in only the Y-direction	The staple has some play, allowing some small movement in the X-direction. Also, the non-spring portion of the rod can undergo a torque with the staple acting as a pivot point.

4.4.3 Convergence

In general FEA will produce an answer for any conditions, however that answer is not necessarily correct. If not enough elements are used, then the program will not be able to correctly represent the underlying problem. As a result, a convergence test must be undertaken to determine if the answer being provided is correct to the precision required. To undertake the convergence test, the accuracy of the element model (mesh) must be increased through refinement and the solutions compared. This process is repeated until the desired precision remains constant.

There are three different methods of refining a finite element model: H-type, P-type and R-type refinement. H-type refinement, is performed by increasing the number of nodes used. P-type refinement, is performed by increasing the order of the equations

used for approximating the solution. And R-type refinement, is performed by rearranging the nodes to have a higher density in areas of high solution gradient

Elements are made of a set number of nodes, so the effect of H-type refinement is to increase the number of elements, P-type refinement increases the number of nodes used per element and R-type refinement makes the elements in the areas of high solution gradient smaller and those in the areas of low solution gradient larger.

In the convergence study of the hysteresis spring bistable mechanism all three forms of refinement were used to a certain extent. H-type refinement was the main mode of refinement used in the convergence study. Each step in the study decreased the spacing between nodes. The highest order shell element appropriate for this type of study was used, starting at the highest level P-type refinement. The smart mesher was used to mesh the layout (place the nodes), which uses a predictive style of R-type refinement that increases the density of the mesh in narrow areas where stresses are more likely to concentrate.

Table 4.3 shows the results of the convergence test at three different Y displacements.

Table 4.3: Data From the Convergence Test

Refinement Level	X (μm)	% Difference From 0.5μm
@ Y = 5μm		
Smart size level 6	3.17397	0.14
Smart size level 1 (finest)	3.18417	0.46
Edge Size 2μ	3.15953	-0.31
Edge Size 1μ	3.16617	-0.10
Edge Size 0.5μ	3.16943	0
@ Y = 10μm		
Smart size level 6	6.67251	0.20
Smart size level 1 (finest)	6.69324	0.51
Edge Size 2μ	6.64047	-0.27
Edge Size 1μ	6.65254	-0.097
Edge Size 0.5μ	6.65902	0
@ Y = 15μm		
Smart size level 6	10.0883	0.11
Smart size level 1 (finest)	10.1137	0.37
Edge Size 2μ	10.0431	-0.32
Edge Size 1μ	10.0641	-0.12
Edge Size 0.5μ	10.0763	0

As summarized in Table 4.3, the percent difference between the highest density mesh (Edge Size 0.5μ) and the lowest density mesh (Smart size level 6) is less than one percent. This change translates to one or more extra digits of accuracy; however, this increase in the level of accuracy in the solution comes at a great cost: approximately 16 times more elements make up the highest density mesh than make up the lowest density mesh. As a result of this increase, the solution time for the highest density mesh was in the order of 90 minutes, where as the solution time for the lowest density mesh was approximately one minute. Because the accuracy difference in the mesh densities is so low in comparison to the error in the input parameters (± ~6 % for Young's Modulus), the lowest density mesh was used for analysis of the different designs in order to save time.

4.4.4 Models Tested

Ten different layouts were converted to ANSYS models and analysed. Three of the ten layouts were included in the proof of concept chip. The other seven H-spring layouts were only modelled. The H-spring layouts are meant to show the effects of changing the strength of the hysteresis spring, the strength of the rod spring and the length of the arm between the hook and the center of rotation for the hysteresis spring. Figure 4.16 gives an example layout for each of the two main design types that were modelled.

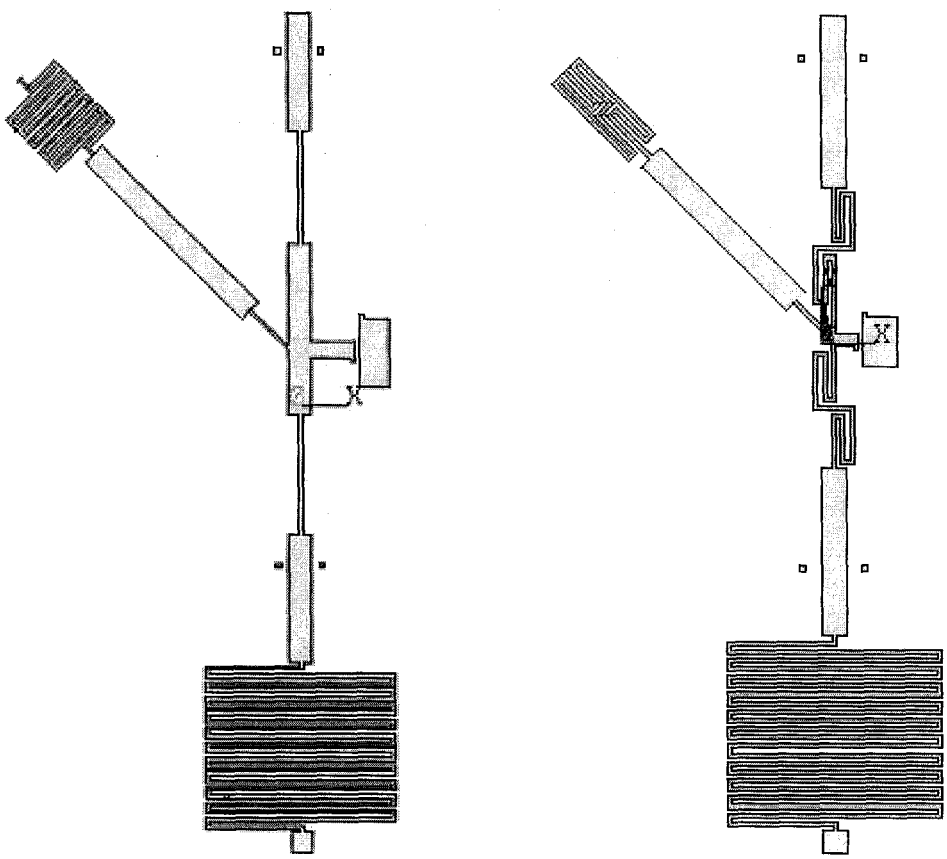

a) b)

Figure 4.16: a) Proof of Concept Design Using Serpentine Hysteresis Springs b) Modelled design using H Style Hysteresis Spring

The main difference between these two designs is the type of springs used. The proof of concept design uses a serpentine spring for the hysteresis spring and a pair of cantilever springs for the lateral rod spring. In comparison, the set of 7 "modelled only" designs use an H-Style spring for the hysteresis spring and a folded spring for the lateral rod spring. The H-spring shown in Figure 4.17 is designed to be significantly stiffer axially than the serpentine spring, while maintaining a low rotational stiffness.

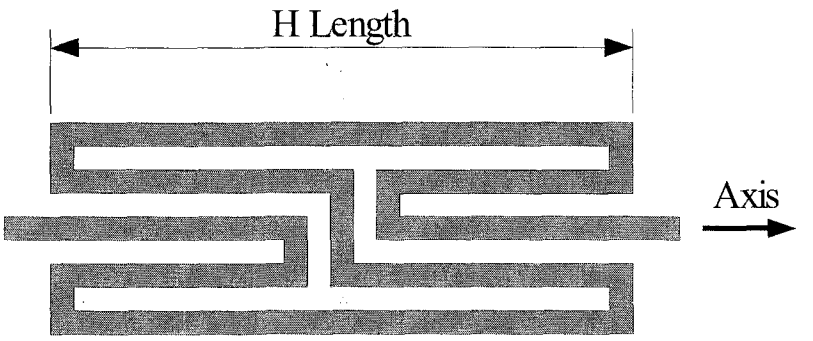

Figure 4.17: H Spring

The axial compliance of a folded spring (inverse of stiffness) is directly proportional to the length of the bars that are parallel to the axis and directly proportional to the cube of the length of the bars that are perpendicular to the axis. Thus, if one desires an axially stiff spring, as much of the spring's length as possible should be made parallel to the spring's axis.

The rotational compliance of a folded spring is directly proportional to the unfolded length of the spring. Thus, to get a larger rotational compliance, or low rotational stiffness, one must add length to the spring.

A straight cantilever has the highest ratio of axial stiffness to rotational stiffness possible because all of its length is parallel to the axis; however, folded springs use chip

space more efficiently than a straight cantilever. Of the folded spring designs, the H-spring has the highest ratio of axial stiffness to rotational stiffness where as the serpentine spring has the lowest. As a result, in future revisions of the design the H-spring will be the spring of choice. This advantage of the H-spring over the serpentine spring is the reason the H-spring was chosen for most of the modelling.

Using a folded spring for the rod spring in the new designs was done to increase the efficiency of the space used in the design. The folding of the spring decreases the stiffness of the rod spring with a minimal penalty on the off axis stiffness and chip area used.

4.4.5 Boundary Conditions

Boundary conditions are how the designer interacts with the finite element model. The boundary conditions create a set of constraints and stimuli that represent how the finite element model interacts with its environment. The first boundary conditions that are attached to the model are the constraints that represent the anchoring of the springs. A boundary condition that enforces no displacement in any direction is applied to the lines that make up the anchor for the returning spring, as shown in Figure 4.18.

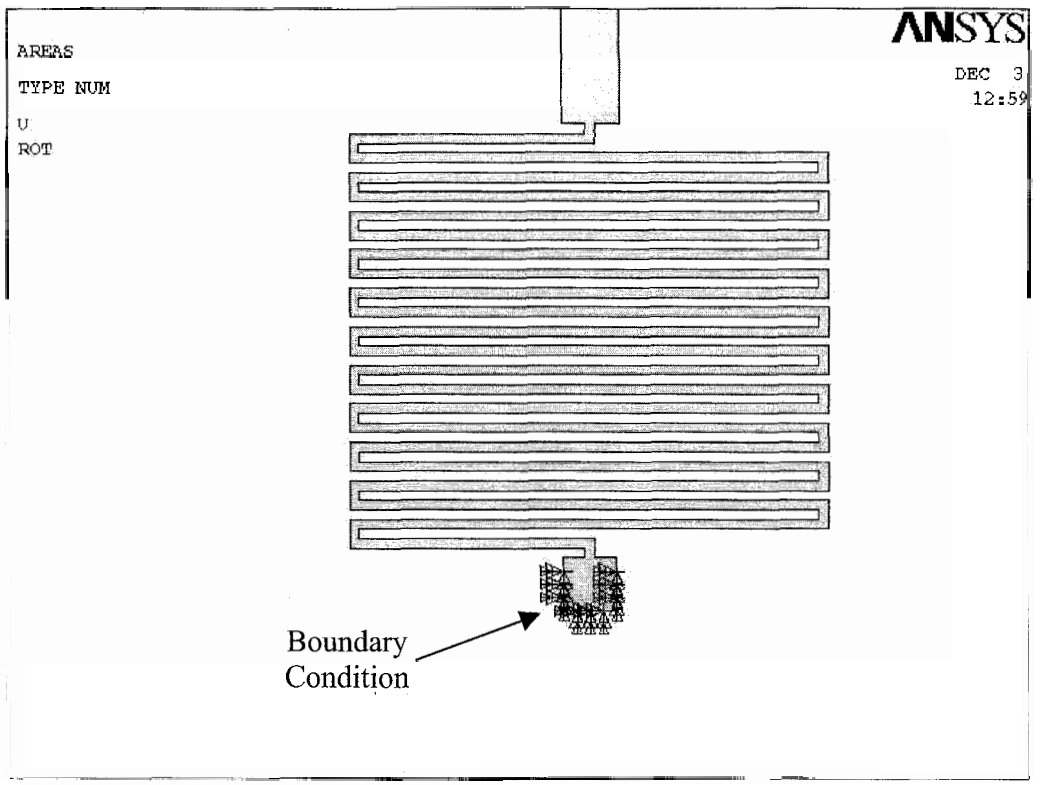

Figure 4.18: Representation of Anchor Boundary Conditions in ANSYS

Because the hysteresis spring is clamped during the actuation phase of operation, a boundary condition equivalent to that of an anchor on the clamped end of the spring is necessary. This zero displacement boundary condition is depicted in Figure 4.19.

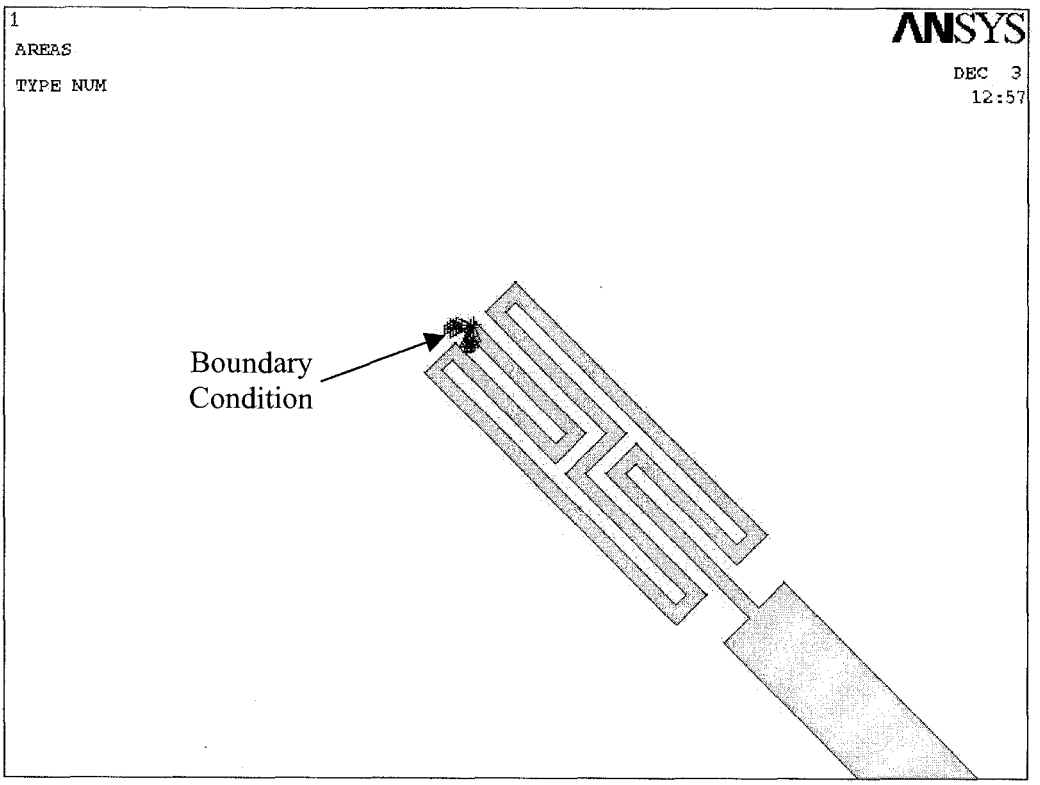

Figure 4.19: Representation of Clamped Anchor Boundary Condition in ANSYS

While the staple anchors are included in the geometric model for visual reference, they are not included in the analysis so as to avoid contact analysis. Contact analysis seeks to model the interactions of parts as they come into contact with each other. Contact analysis is highly non-linear and requires significantly larger solution times. As well, contact analysis can result in an analysis being unable to mathematically converge, which provides unusable solutions. Thus, to avoid the difficulties presented by contact analysis, the staples are represented by a constraint that allows the non-spring portions of the rod to move in only the Y direction. This constraint is essentially modelling the staples as an ideal sliding joint. The staple constraints are depicted in Figure 4.20.

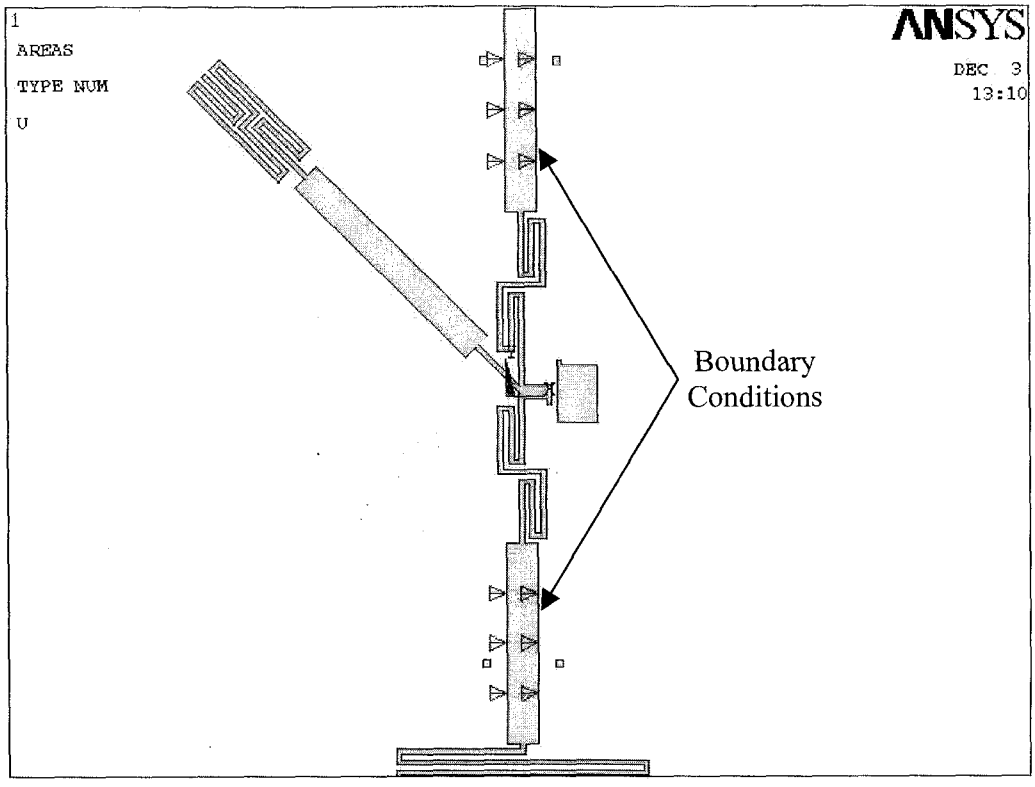

Figure 4.20: Representation of Staple Constraints in ANSYS

One of the assumptions made to simplify the analysis was to prohibit out-of-plane interactions. While some out of plane buckling and torsion occurs in MEMS devices, such out of plane interactions were not considered in this analysis. Removing out of plane interactions was accomplished though the use of a boundary condition on every node that set displacement in the Z direction to zero. Ignoring out of plane interactions had two benefits with respect to the analysis. Firstly, this simplification reduced the solution time by removing one degree of freedom from every node. Secondly, the simplification made the analysis more mathematically stable. Without the boundary condition removing displacement in the Z direction, the large Y displacement cases would not mathematically converge.

The final boundary condition to add is the condition representing actuation. Displacement boundary conditions of 5μm, 10μm and 15μm, were applied to the end of the rod where the actuation block would be added. The placement of the actuation boundary condition is illustrated in Figure 4.21.

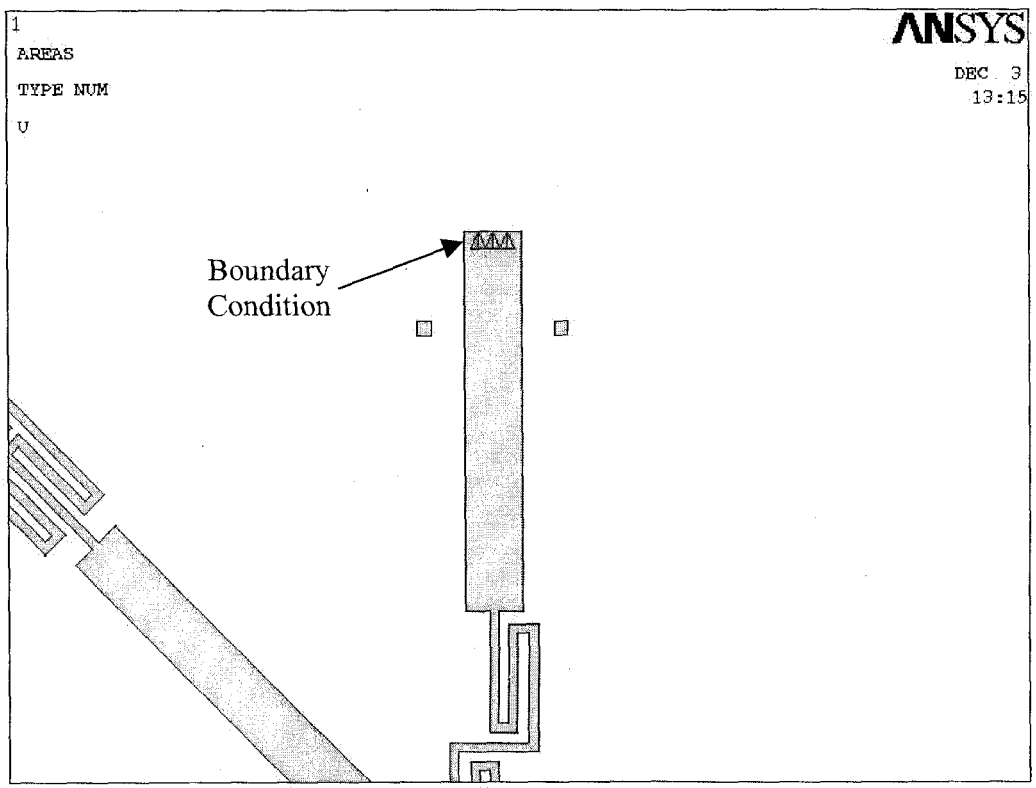

Figure 4.21: Representation of Actuation Boundary Condition in ANSYS

5 RESULTS AND DISCUSSION

5.1 Fabrication Results

A proof of concept design was designed and fabricated using the polyMUMPS® process. This three layer polysilicon process was provided free of charge though the Canadian Microelectronics Corporation (CMC) as a grant. The provision of 0.5 mm x 0.5 mm in chip space was invaluable to this work. The basic layout of the fabricated devices is shown in Figure 5.1.

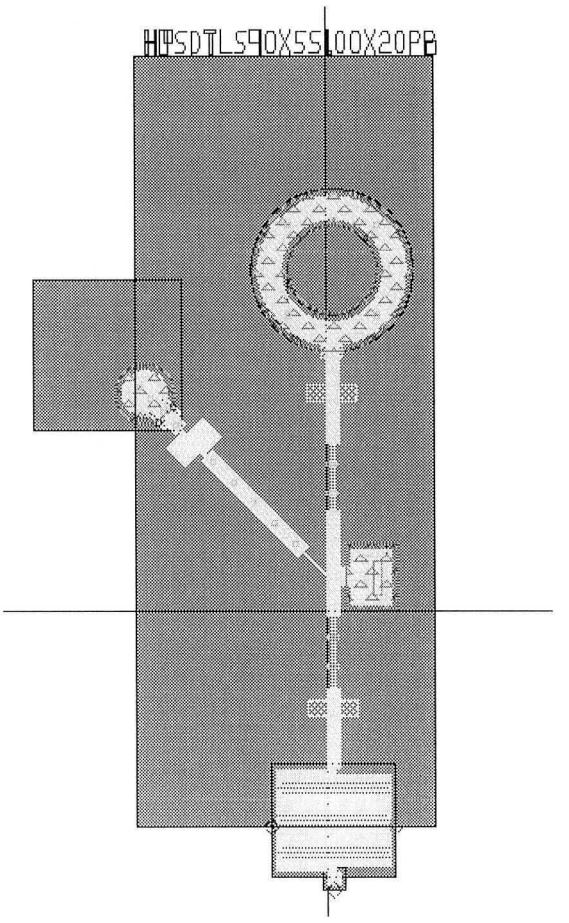

Figure 5.1: Basic Layout of the Hysteresis Bistable Mechanism

The pad and ring were designed to anchor the hysteresis spring and actuate the rod.

The hook and latch were made double thickness in order to improve the reliability of the contact between the two. When contacting parts are made single thickness, the likelihood that the parts will slip past each other due to out of plane movement is increased. Although the staples are theoretically meant to constrain out of plane movement, practically a nominal play of 2.0μm can occur before the staple can constrain out of plane movement. Because a single thickness layer is nominally 2.0μm, the likelihood of two single thickness parts contacting solidly is lower than two double thickness parts, which have a nominal thickness of 3.5μm. Figure 5.2 shows a Scanning Electron Micrograph (SEM) of a double thickness hook and latch.

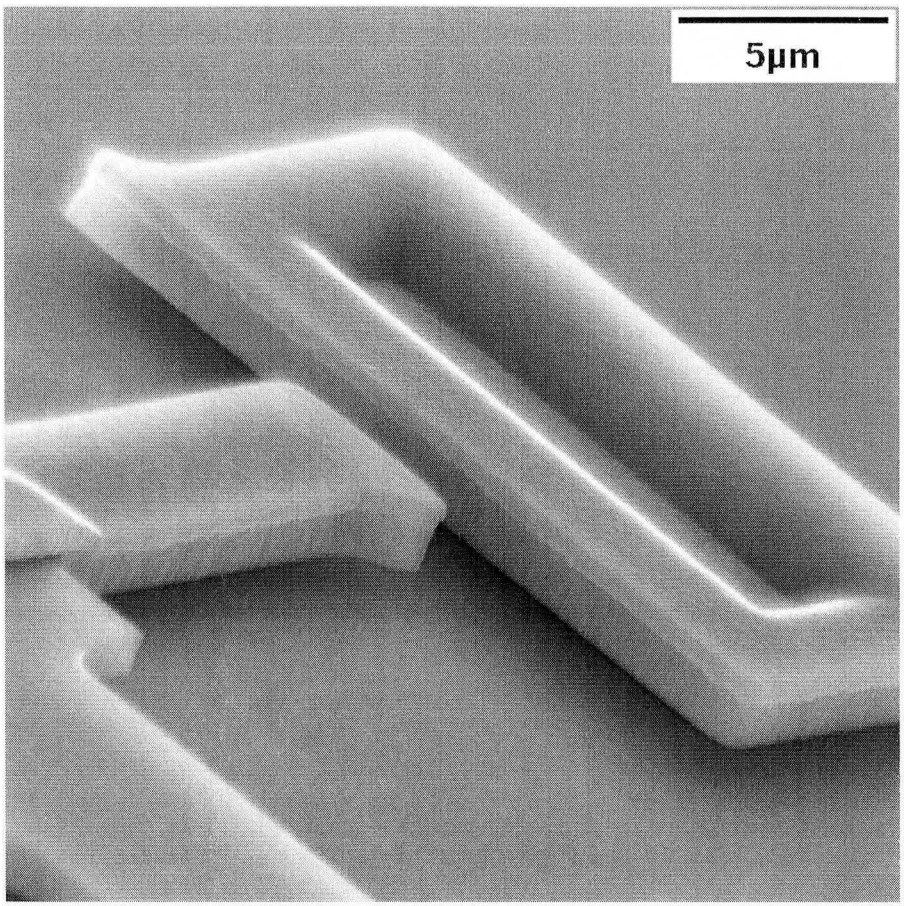

Figure 5.2: SEM of a Double Thickness Hook and Latch

The springs chosen for the proof of concept design were serpentine springs. Unfortunately, these springs were chosen using the simple model that, after further analysis, turned out to be quite inaccurate. As a result, springs operated outside of their linear region, which resulted in more lateral movement than predicted by the improved rotational model. This extra lateral movement was beneficial as the original simple model overestimated the lateral movement. If the springs had not left linear operation, enough lateral movement to allow latching would not have been present. As a result of the non-linear operation of the springs, the fabricated devices operate as described in section 4.2. Figure 5.3 shows an SEM of the devices as fabricated.

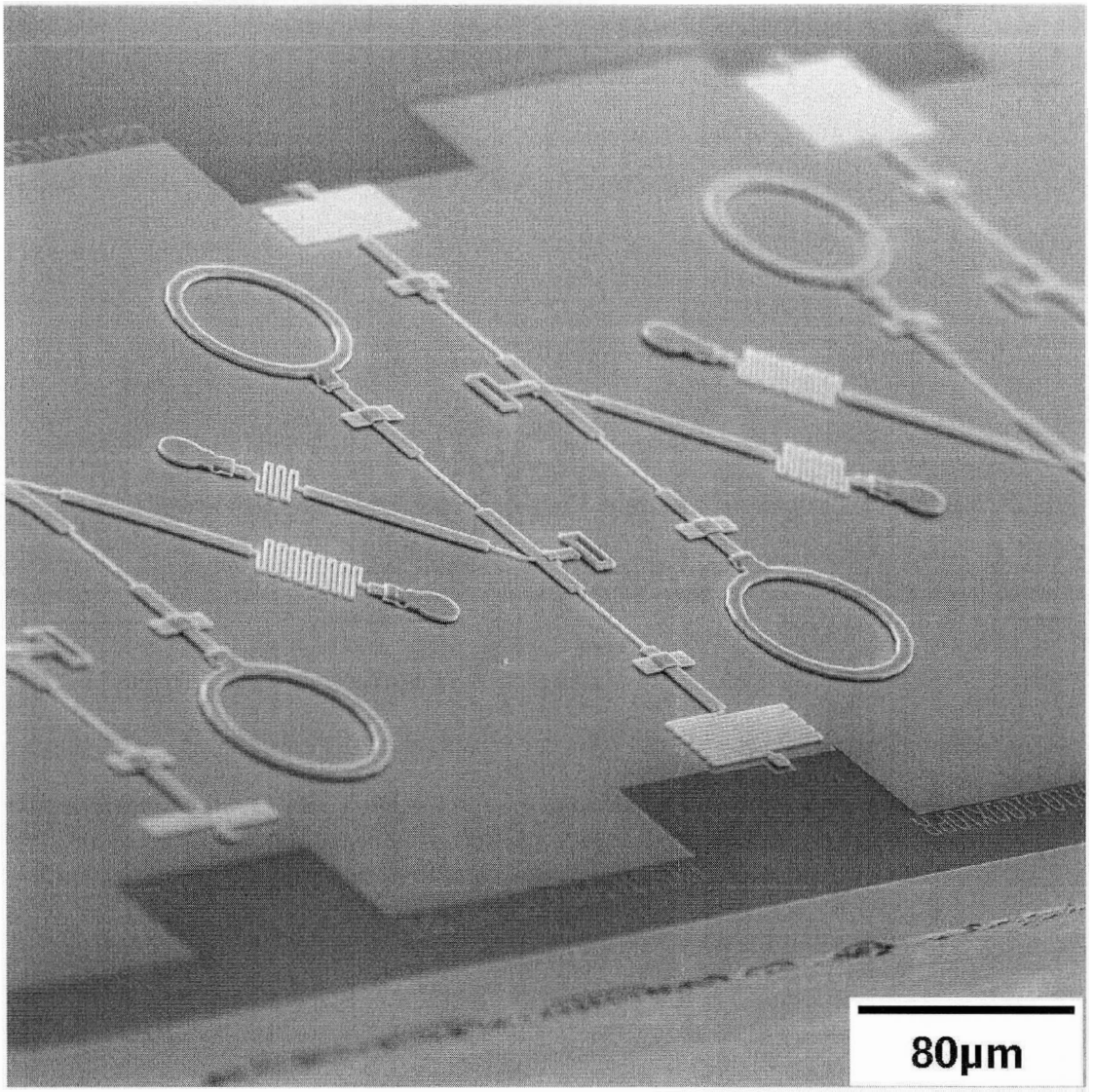

Figure 5.3: SEM of a Complete Device

Figure 5.4 shows an optical photograph of a functioning device in its unlatched and latched states.

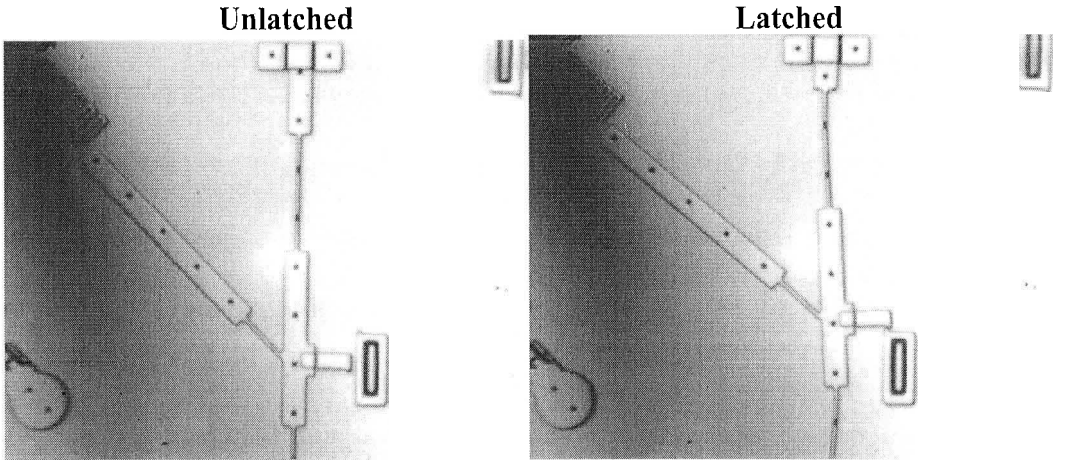

Figure 5.4: Optical Photograph of Unlatched and Latched States

Appendix 7.1 includes the frames of a movie showing a functioning device.

5.2 Comparison of Models and Results

The first comparison made is between the rotational analytical model and the finite element model. This comparison will verify if the two modelling methods agree with each other. The next comparison is between the two modelling methods and the results of fabrication. This comparison will verify if the two modelling methods agree with reality.

5.2.1 Comparison of Models

The H-spring style layout was used to compare the rotational analytical model and the finite element model. The serpentine spring style layout was also tested and those results are presented in section 5.2.2. The values of the three design parameters were permuted around a center value of: H-spring length 50μm, L length of 150μm and a Rod spring length of 25μm.

The H-spring length parameter changes both the $K_{HystAxial}$ and $\beta_{HystRotational}$ because even though the model separates the hysteresis spring into two different springs, the reality is that one spring is present and the rotational and axial spring constants are related by the spring design chosen. Figure 5.5 shows how the H-spring length parameter relates to the layout of an H-spring.

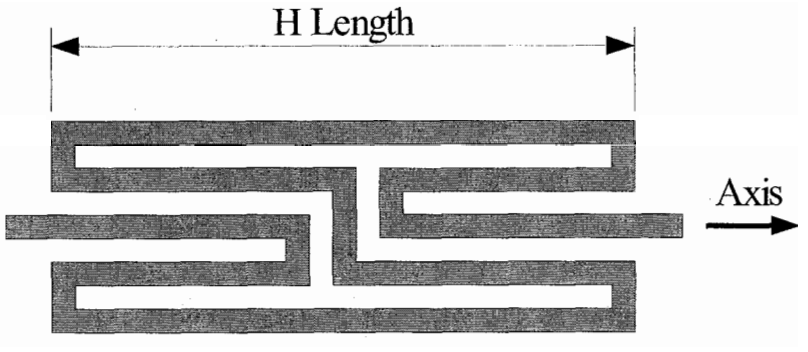

Figure 5.5: H-spring Length Parameter

The L parameter is the L described in the analytical model. That is, L is the initial rest length of the hysteresis spring from the center of rotation to the attachment point with the hook. This length includes the rod that connects the H-spring to the attachment point with the hook.

The rod spring length changes the value of K_{Rod} only. Figure 5.6 shows how the R-spring length parameter relates to the layout of the rod springs.

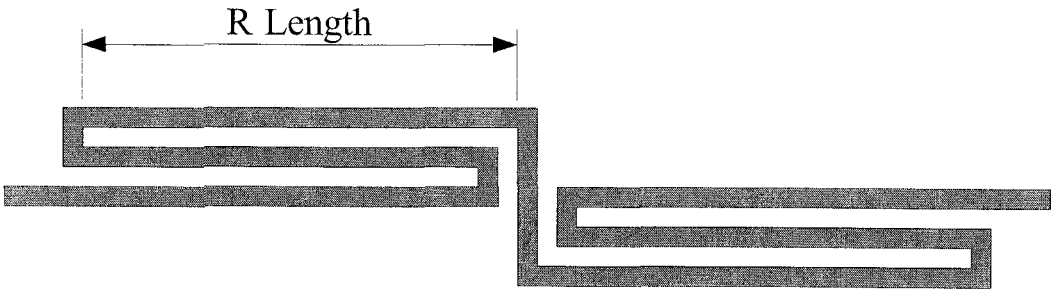

Figure 5.6: Rod Spring Length Parameter

Two rod springs are present in the layouts: one above the hook and one below. Both of these rod springs have the same R length parameter.

The case names contain the values of the three design parameters used in that case. For example, the center case is H50L150R25, the H50 indicates that an H length parameter of 50μm was used, the L150 indicates that an L length parameter of 150μm was used and the R25 indicates that an R length parameter of 25μm was used. Table 5.1 gives a list of the cases that were modeled both analytically and though FEA.

Table 5.1: Cases Considered in Model Comparison

Case Name	H Length (μm)	L Length (μm)	R Length (μm)
H50L150R25	50	150	25
H25L150R25	25	150	25
H75L150R25	75	150	25
H50L100R25	50	100	25
H50L200R25	50	200	25
H50L150R20	50	150	20
H50L150R30	50	150	30

The studied cases permute each parameter around the center case of H50L150R25. The first parameter permuted is the H-spring length. Table 5.2 gives the

values of the X displacement for a given H-spring length parameter at three different Y displacements.

Table 5.2: Comparison of H Length Permutation Results At Three Different Y Displacements

Case	FEA Result	Analytical Result	% Difference
		Y @ 5μm	
H25L150R25	3.174E-06	3.482E-06	-9.71
H50L150R25	2.679E-06	2.771E-06	-3.42
H75L150R25	2.211E-06	2.299E-06	-3.94
		Y @ 10μm	
H25L150R25	6.673E-06	6.793E-06	-1.80
H50L150R25	5.247E-06	5.456E-06	-3.97
H75L150R25	4.192E-06	4.552E-06	-8.60
		Y @ 15μm	
H25L150R25	1.009E-05	9.926E-06	1.61
H50L150R25	7.945E-06	8.041E-06	-1.21
H75L150R25	5.132E-06	6.747E-06	-31.48

The next parameter permuted is the L length. Table 5.3 gives the values of the X displacement for a given L length parameter at three different Y displacements.

Table 5.3: Comparison of L Length Permutation Results At Three Different Y Displacements

Case	FEA Result	Analytical Result	% Difference
		Y @ 5μm	
H50L100R25	2.632E-06	2.697E-06	-2.48
H50L150R25	2.679E-06	2.771E-06	-3.42
H50L200R25	2.953E-06	2.800E-06	5.18
		Y @ 10μm	
H50L100R25	5.257E-06	5.266E-06	-0.16
H50L150R25	5.247E-06	5.456E-06	-3.97
H50L200R25	5.516E-06	5.537E-06	-0.38
		Y @ 15μm	
H50L100R25	7.670E-06	7.679E-06	-0.12
H50L150R25	7.945E-06	8.041E-06	-1.21
H50L200R25	8.066E-06	8.202E-06	-1.68

The last parameter permuted is the rod spring length. Table 5.4 gives the values of the X displacement for a given rod spring length parameter at three different Y displacements.

Table 5.4: Comparison of R Length Permutation Results At Three Different Y Displacements

Case	FEA Result	Analytical Result	% Difference
		Y @ 5μm	
H50L150R20	2.066E-06	1.988E-06	3.77
H50L150R25	2.679E-06	2.771E-06	-3.42
H50L150R30	3.154E-06	3.350E-06	-6.23
		Y @ 10μm	
H50L150R20	4.208E-06	3.951E-06	6.11
H50L150R25	5.247E-06	5.456E-06	-3.97
H50L150R30	6.270E-06	6.547E-06	-4.42
		Y @15μm	
H50L150R20	5.674E-06	5.877E-06	-3.57
H50L150R25	7.945E-06	8.041E-06	-1.21
H50L150R30	9.403E-06	9.583E-06	-1.91

The data in Table 5.2 through Table 5.4 indicates that the analytical model and the finite element models agree within ±10% with the exception of case H75L150R25 in Table 5.2, which had a percent difference of -31.48% at a Y displacement of 15μm. However, the finite element modeling was done using large displacement effects, which are non-linear changes in the parameters of an object when its geometric shape is "greatly changed". In the case of this study, these large displacement effects manifest themselves as non-linear spring constants. When a cantilever beam tip deflects ~10% of the beam's length, then non-linear effects begin to become significant. The analytical model assumes that all the springs are linear therefore to determine if this outlier was caused by the non-linear effects, the case H75L150R25 was put through FEA with the large displacement effects turned off. This new FEA result was within -1.98% of the analytical solution.

A few sources of error contribute to the differences between the analytical models and the finite element models. One major source of error is that the analytical model does not take into account the large displacement effects, as seen in case H75L150R25.

A second possible source of error is in the calculation of the spring constants for the analytical model. A third possible source of error is the simplifying assumptions made in the development of the analytical model.

As long as large displacement effects are avoided the analytical model agrees within ±10% of the finite element models. Also note that a great deal of overhead work must be undertaken when performing FEA. Although the solution time for each FEA was in the order of a few minutes, the actual simulation required approximately an hour in order to create the geometric model, import the model to ANSYS®, mesh the model and attach boundary conditions. The analytical model took less than a minute to run all of the cases. Because the analytical model is solved within seconds rather than the hour required for a finite element model, the analytical model could be used as a screening method to determine which permutations are worth modeling using FEA.

The analytical model could have great use as a tool for first approximations. The analytical model should be further developed to identify the main sources of error in order to minimize the errors, or, at least have a better idea of which calculations are likely to be error prone.

5.2.2 Models versus Reality

To compare the fabricated results to the two models, three of the layouts were converted into ANSYS® format. The proof of concept design only permuted the hysteresis spring and the return spring strengths. Because the return spring does not affect the relationship between Y and X displacements, only the three hysteresis spring permutations were considered. The serpentine springs used in the design all had the same

bar length of 40μm and the spring constant was permuted by changing the numbers of bars ganged together. The three cases had 5, 10 and 15 bars respectively.

Before comparing the models to the fabrication results, the two modeling techniques were again compared to determine if they still agree with each other when using a different spring type. The results of the analytical and finite element models are given in Table 5.5.

Table 5.5: Comparison of Bar Number Permutation Results At Three Different Y Displacements

Case	FEA Result	Analytical Result	% Difference
		Y @ 5μm	
N = 5	7.147E-07	6.805E-07	4.78
N = 10	4.266E-07	3.752E-07	12.04
N = 15	2.956E-07	2.590E-07	12.40
		Y @ 10μm	
N = 5	1.441E-06	1.369E-06	5.03
N = 10	8.677E-07	7.561E-07	12.86
N = 15	6.030E-07	5.223E-07	13.39
		Y @ 15μm	
N = 5	2.169E-06	2.062E-06	4.91
N = 10	1.309E-06	1.142E-06	12.76
N = 15	8.871E-07	7.892E-07	11.04

The results in Table 5.5 show the difference between the two modeling methods growing to ~12%. This may be due to the accuracy of the spring constant calculations, as the calculations for the H-spring and serpentine spring are different.

These proof of concept layouts were designed only to work. Because they were not designed for verifying the models, acquiring accurate measurements with our available test set-ups was impossible. However, using pictures taken during the verification of the device's functionality, an estimate of the X displacement at a Y

displacement of 25μm was possible. The values obtained, as well as the predictions of the analytical model, are summarized in Table 5.6.

Table 5.6: Fabrication Results Compared to Analytical Results

Case	Fabrication Result	Analytical Result	% Difference
		Y @ 25μm	
N = 5	~12	3.5	70
N = 10	~7	1.9	72
N = 15	~6	1.3	78

As summarized in Table 5.6, the fabrication results and the analytical results do not agree. The proof of concept layouts required 4μm of X displacement at 25μm of Y displacement in order to latch. The analytical model predicts that none of the designs should have worked, but they all did. The main reason for this disparity between results and prediction is that the springs used deformed too much and the bars came into contact with each other. When the bars came into contact with each other, the spring acted like a solid lump, not a spring, and a jump discontinuity in the spring constant occurred. Neither the analytical model nor the finite element model used could take this contact into account. Thus, they provide a prediction of performance that is incorrect.

While the results of the contact cannot be handled using the current finite element model, the contact can be predicted as the spring can be clearly seen to pass through itself, as shown in Figure 5.7.

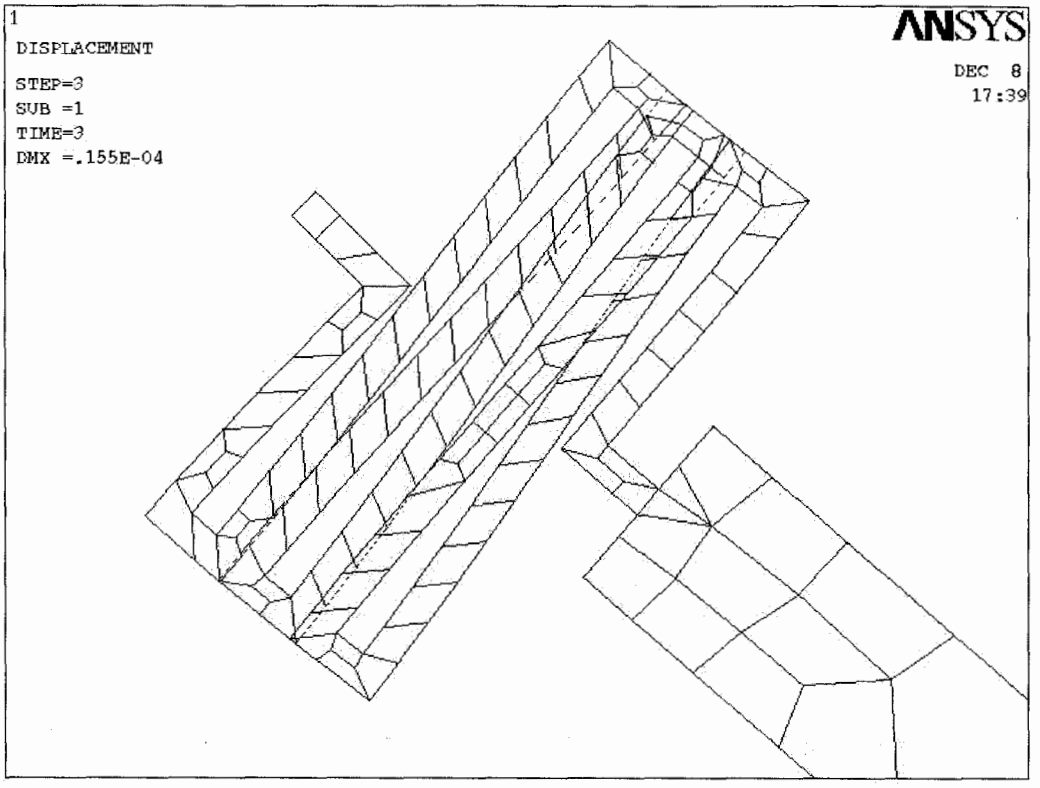

Figure 5.7: Spring Bars Interfering With Each Other

Including contact in the finite element model is possible, however, adding contact analysis to the springs would be even more complex than adding it for the latch. See section 4.4.5 for further discussion of contact analysis in finite element modeling.

Even if the hysteresis spring does not contact itself, error in the prediction may occur because of the simplifying assumptions made in the development of the models. One such assumption, likely to affect the predictions, is that the staple is not perfect in confining the rod in the X direction. Horizontal play in the staple would manifest itself as constant offset in the X direction, as the rod spring will not engage until the staple confines the rod. Unfortunately, such improvements to the model are not possible with the current layouts. In fact, the current fabricated devices are not sufficient to verify the

validity of or improve the models, because the fabricated devices were not designed to be used for verification of the models. The devices were designed only to prove the functional concept. Thus, while the models seem to agree with each other, further work is needed to truly verify both of the models through further comparison with each other and through the design of a new set of layouts, created with the verification of the models as the prime objective.

6 CONCLUSION

A bistable mechanism is an important building block for many MEMS applications. This thesis has presented the first reported single digital input bistable MEMS mechanism. This work developed the hysteresis spring as an enabling mechanism to allow the creation of the first reported single digital input bistable mechanism. The functionality of the hysteresis spring single digital input bistable mechanism has been described in detail. As well, a model of the latching functionality was developed using analytical techniques. The analytical model agreed within an acceptable range of the results of finite element modeling when the springs operate in their linear region. However, the proof of concept design was fabricated and the devices demonstrated the prescribed functionality.

Further work should be undertaken to fine-tune the models and verify their agreement with the experimental results. To this end, a set of designs that match the modeled cases should be fabricated and their performance be compared to the results of finite element analysis. Further work should also be undertaken to determine the best actuators to be used for both actuation in the Y direction and clamping of the hysteresis spring's anchor. Enhanced actuation would allow switching speed and reliability studies to be performed.

7 APPENDICES

7.1 Functional Movie

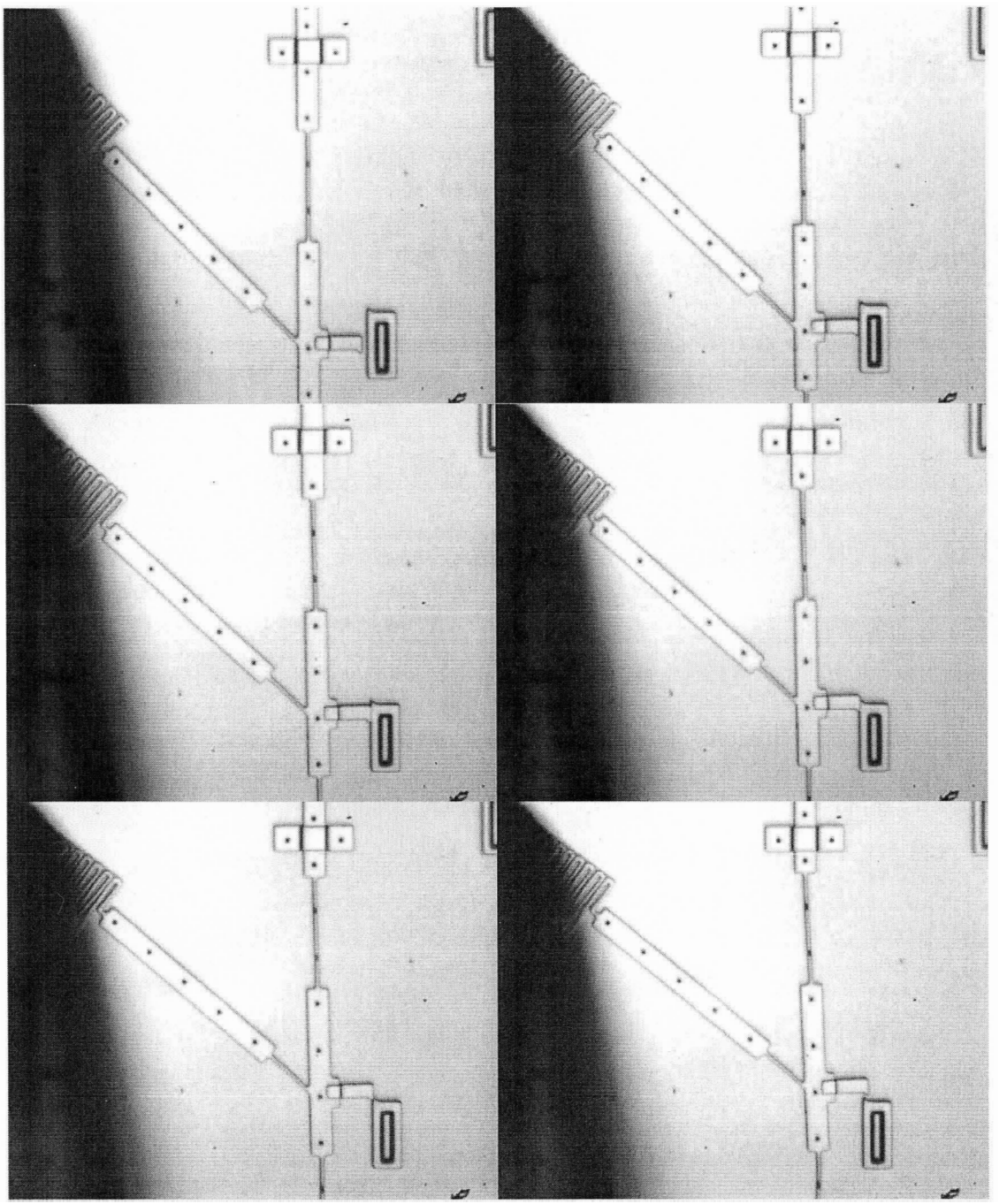

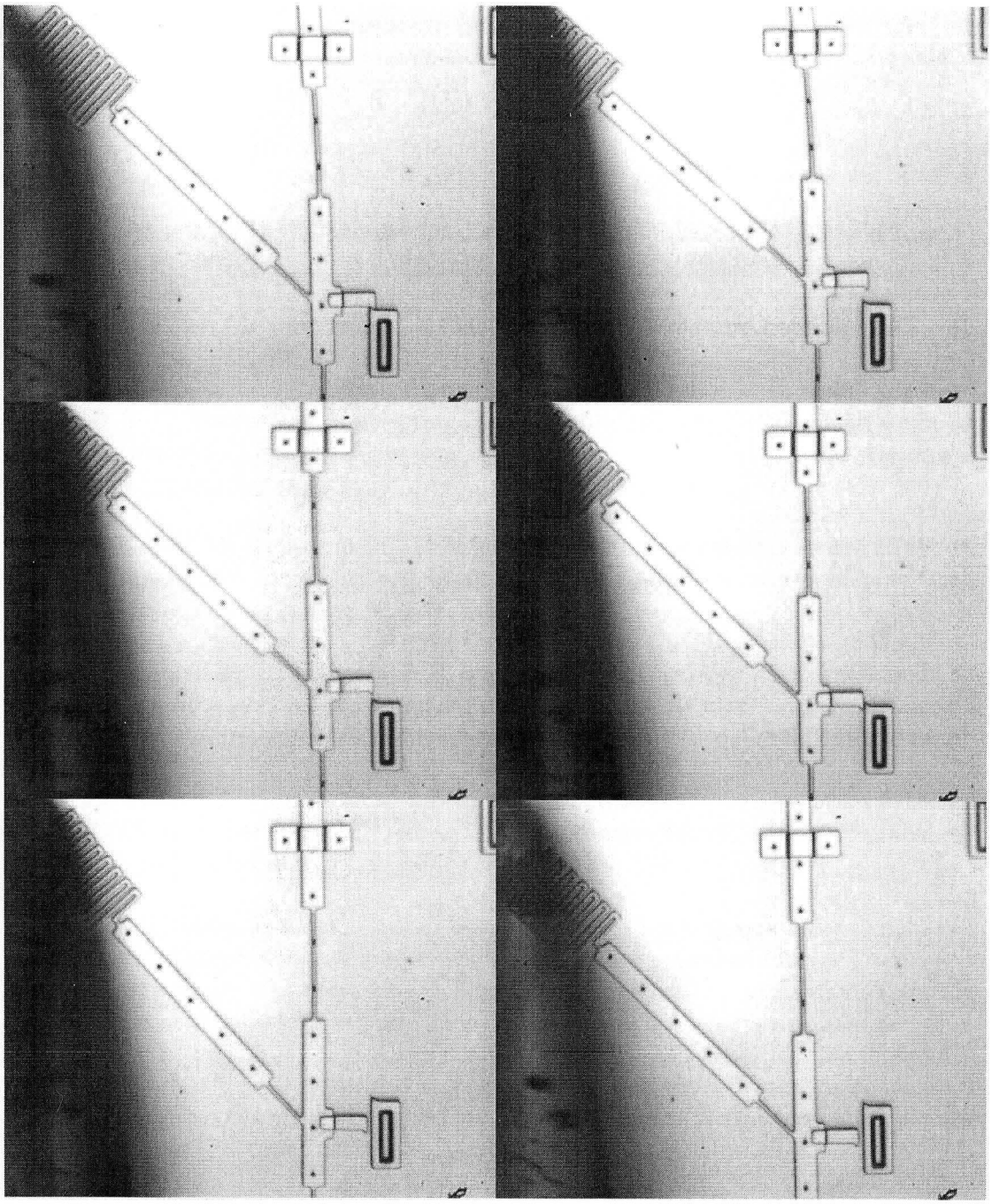

8 REFERENCES

[1] AllAboutMEMS, "allaboutmems.com - What is MEMS > MEMS Applications." January 2004: http://allaboutmems.com/memsapplications.html.

[2] K. E. Petersen, "Silicon as a mechanical material," *Proceedings of the IEEE*, vol. 70, pp. 420-57, 1982.

[3] B. Y. U. Mechanical Engineering Group, "Introduction to Bistable Compliant Mechanisms." January 2004: http://research.et.byu.edu/llhwww/special/bistable.html.

[4] P. Kopka, M. Hoffmann, and E. Voges, "Micromechanical fiber switch arrays on silicon," presented at Proceedings of ECOC '98 - 24th European Conference on Optical Communication, Madrid, Spain, 1998.

[5] L. A. Field, D. L. Burriesci, P. R. Robrish, and R. C. Ruby, "Micromachined 1*2 optical fiber switch," presented at Proceedings of the International Solid-State Sensors and Actuators Conference - TRANSDUCERS `95, Stockholm, Sweden, 1995.

[6] E. Ollier, P. Labeye, and F. Revol, "Micro-opto mechanical switch integrated on silicon," *Electronics Letters*, vol. 31, pp. 2003-5, 1995.

[7] M. Hoffmann, P. Kopka, and E. Voges, "Lensless latching-type fiber switches using silicon micromachined actuators," presented at Optical Fiber Communication Conference. Technical Digest Postconference Edition. Trends in Optics and Photonics Vol.37, 2000.

[8] M. Hoffmann, P. Kopka, and E. Voges, "All-silicon bistable micromechanical fiber switch based on advanced bulk micromachining," *IEEE Journal of Selected Topics in Quantum Electronics*, vol. 5, pp. 46-51, 1999.

[9] M. Hoffmann, P. Kopka, and E. Voges, "Bistable micromechanical fiber-optic switches on silicon," presented at 1998 IEEE/LEOS Summer Topical Meeting. Broadband Optical Networks and Technologies: An Emerging Reality. Optical MEMS. Smart Pixels. Organics Optics and Optoelectronics, 1998.

[10] M. Hoffmann, P. Kopka, T. Gross, and E. Voges, "All-silicon bistable micromechanical fibre switches," *Electronics Letters*, vol. 34, pp. 207-8, 1998.

[11] P. Kopka, M. Hoffmann, and E. Voges, "Bistable 2*2 and multistable 1*4 micromechanical fibre-optic switches on silicon," presented at Proceedings of MOEMS 99, Mainz, Germany, 1999.

[12] T. Y. Chai, T. H. Cheng, S. K. Bose, C. Lu, and G. Shen, "Array interconnection for rearrangeable 2-D MEMS optical switch," *Journal of Lightwave Technology*, vol. 21, pp. 1134-40, 2003.

[13] G. Shen, T. H. Cheng, S. K. Bose, C. Lu, and T. Y. Chai, "Architectural design for multistage 2-D MEMS optical switches," *Journal of Lightwave Technology*, vol. 20, pp. 178-87, 2002.

[14] S.-S. Lee, L.-S. Huang, C.-J. Kim, and M. C. Wu, "Free-space fiber-optic switches based on MEMS vertical torsion mirrors," *Journal of Lightwave Technology*, vol. 17, pp. 7-13, 1999.

[15] Y. Kato, K. Mori, T. Mase, A. Takahashi, O. Imaki, and R. Kaku, "Development of 4*4 MEMS optical switch," presented at 2000 IEEE/LEOS International Conference on Optical MEMS, Kauai, HI, USA, 2000.

[16] A. Q. Liu, X. M. Zhang, and Y. L. Lam, "A high performance 4*4 free-space fiber-optic crossconnection," presented at 2000 IEEE/LEOS International Conference on Optical MEMS, Kauai, HI, USA, 2000.

[17] R. L. Wood, R. Mahadevan, and E. Hill, "MEMS 2D matrix switch," presented at Optical Fiber Communications Conference (OFC), Anaheim, CA, USA, 2002.

[18] K. Bergman, "Overview of high capacity optical cross-connects," presented at LEOS 2001. 14th Annual Meeting of the IEEE Lasers and Electro-Optics Society, 2001.

[19] T. Yamamoto, J. Yamaguchi, N. Takeuchi, A. Shimizu, E. Higurashi, R. Sawada, and Y. Uenishi, "A three-dimensional MEMS optical switching module having 100 input and 100 output ports," *IEEE Photonics Technology Letters*, vol. 15, pp. 1360-2, 2003.

[20] Y. Uenishi, J. Yamaguchi, T. Yamamoto, N. Takeuchi, A. Shimizu, E. Higurashi, and R. Sawada, "Free-space optical cross connect switch based on a 3D MEMS mirror array," presented at LEOS 2002. 2002 IEEE/LEOS Annual Meeting Conference Proceedings. 15th Annual Meeting of the IEEE Lasers and Electro-Optics Society, Glasgow, UK, 2002.

[21] L. Latorre, J. Kim, J. Lee, P.-P. de Guzman, H. J. Lee, P. Nouet, and C.-J. Kim, "Electrostatic actuation of microscale liquid-metal droplets," *Journal of Microelectromechanical Systems*, vol. 11, pp. 302-8, 2002.

[22] X.-Q. Sun, K. R. Farmer, and W. N. Carr, "A bistable microrelay based on two-segment multimorph cantilever actuators," presented at Proceedings IEEE Eleventh Annual International Workshop on Micro Electro Mechanical Systems An Investigation of Micro Structures, Sensors, Actuators, Machines and Systems, Heidelberg, Germany, 1998.

[23] M. Ruan, J. Shen, and C. B. Wheeler, "Latching micro magnetic relays with multistrip permalloy cantilevers," presented at Technical Digest. MEMS 2001. 14th IEEE International Conference on Micro Electro Mechanical Systems, Interlaken, Switzerland, 2001.

[24] B. D. Jensen, M. B. Parkinson, K. Kurabayashi, L. L. Howell, and M. S. Baker, "Design optimization of a fully-compliant bistable micro-mechanism," presented at Micro-Electro-Mechanical Systems (MEMS). 2000 ASME International Mechanical Engineering Congress and Exposition, New York, NY, USA, 2001.

[25] J. Qiu, J. H. Lang, and A. H. Slocum, "A centrally-clamped parallel-beam bistable MEMS mechanism," presented at Technical Digest. MEMS 2001. 14th IEEE International Conference on Micro Electro Mechanical Systems, Interlaken, Switzerland, 2001.

[26] J. Qui, J. H. Lang, A. H. Slocum, and R. Strumpler, "A high-current electrothermal bistable MEMS relay," presented at Proceedings IEEE Sixteenth Annual International Conference on Micro Electro Mechanical Systems, Kyoto, Japan, 2003.

[27] H. Matoba, T. Ishikawa, C.-J. Kim, and R. S. Muller, "A bistable snapping microactuator," presented at Proceedings IEEE Micro Electro Mechanical Systems An Investigation of Micro Structures, Sensors, Actuators, Machines and Robotic Systems, Oiso, Japan, 1994.

[28] B. D. Jensen, L. G. Salmon, and L. L. Howell, "Design of two-link, in-plane, bistable compliant micro-mechanisms," *Journal of Mechanical Design*, vol. 121, pp. 416-423, 1999.

[29] I. Foulds, N. Trinh, S. Hu, S. Liao, R. Johnstone, and X. Parameswaran, "A surface micromachined bistable switch," presented at IEEE CCECE2002. Canadian Conference on Electrical and Computer Engineering. Conference Proceedings, Winnipeg, Man., Canada, 2002.

[30] I. G. Foulds, M. T. Trinh, S. Hu, S. W. Liao, R. W. Johnstone, and M. A. Parameswaran, "New design for surface micromachined bistable and multistable switches," *Journal of Microlithography, Microfabrication, and Microsystems*, vol. 2, pp. 255-8, 2003.